Title: Mucosal BCG vaccination reprograms lung interstitial macrophages and enhances antimicrobial defense in mice

Authors: Aaron James Forde[1,8]*, Mara Esposito[1]*, Emanuela Kerschbamer[1]*, David Schreiner[1], Eduardo Moreo[1], Nikos Pantouloufos[1], Tiphaine MN Camarasa[1], Jean de Lima[1], Habiba Soliman[1], Maike Erber[1], Claire E. Depew[1], Wadschma Naderi[1] and Carolyn G. King[1,8].

[1]: Infection Immunology Laboratory, Department of Biomedicine, University of Basel, Basel, CH 4058, Switzerland.

[8]: Lead contacts.

***These authors contributed equally.**

Corresponding authors:

Aaron J. Forde and Carolyn G. King

Department of Biomedicine

University of Basel

Mattenstrasse 28

CH-4058 Basel, Switzerland

Email: aaronjames.forde@unibas.ch; carolyn.king@unibas.ch

Tel: +41 61 207 5080 (AJF); +41 78 907 15 68 (CGK)

Abstract:

Bacille Calmette–Guérin (BCG) is the only licensed vaccine against tuberculosis (TB) but provides inconsistent protection against disease. Studies in non-human primates show that intravenous BCG confers superior protection compared to intradermal vaccination, yet how different vaccination routes reprogram lung immunity in mice - the primary model for mechanistic studies - remains incompletely defined at single cell or spatial resolution. Moreover, while lung macrophages are key effectors during *Mycobacterium tuberculosis* infection, most studies have focused on alveolar macrophages, leaving interstitial macrophage responses to vaccination largely unexplored. Here, we define the cellular and spatial immune landscape shaped by three BCG vaccination routes in mice using flow cytometry, single-cell RNA sequencing, and spatial transcriptomics. Comparing intratracheal (IT), intravenous (IV), and subcutaneous (SC) vaccination, we demonstrate that mucosal IT delivery uniquely reprograms interstitial macrophages, establishes spatially organized immune hubs with CD4 T cells, and provides superior protection against infectious challenge. These findings identify IM as key mediators of mucosal vaccine-induced protection and provide a framework for the rational optimization of vaccines against respiratory pathogens.

Introduction

Tuberculosis (TB) remains one of the world's deadliest infectious diseases, causing an estimated 10.8 million cases and 1.25 million deaths in 2023, with the highest burden in resource limited low- and middle-income countries (1). Despite widespread use for over a century, Bacillus Calmette-Guérin (BCG) remains the only licensed vaccine against TB and provides inconsistent protection against pulmonary disease. A deeper understanding of the immune mechanisms underlying durable protection is urgently needed.

Lung macrophages are among the first immune cells to encounter *Mycobacterium tuberculosis* (Mtb), the causative agent of TB, following inhalation. Two major macrophage subsets inhabit the lung: alveolar macrophages (AM), which reside in the airspaces, and interstitial macrophages (IM), which occupy the lung parenchyma (2). These macrophages differ in origin, metabolic state and antimicrobial capacity. AM are the earliest responders to Mtb, and accumulating evidence suggests that prior vaccination can metabolically and epigenetically reprogram them to restrict Mtb growth, ultimately reducing early bacterial burden and shaping the trajectory of disease progression (3,4). In comparison, the precise nature of IM rewiring following BCG vaccination is less well understood. Surface marker expression levels of CD206, CD11c, MHCII, Lyve1, CX3CR1 and CD169 have been used by different groups in an effort to further describe IM heterogeneity in the naive lung (5–7). Additional work to better characterize different subgroups of IM has shown a distinct functional separation based on expressed chemokines (8). However, how IM might be modulated during infection remains largely unknown. Importantly, IM are not a static population: upon niche depletion, Ly6c high monocytes undergo local differentiation into IM in an M-CSF, MafB and TGFβ dependent manner, suggesting that the IM compartment retains plasticity and could be exploited by vaccination (9,10). Moreover, evidence suggests that the role of IM during pulmonary infection may be context dependent. For example, IM have been shown to be permissive to *Klebsiella pneumoniae* and depletion of IM in a fungal infection model resulted in significantly reduced pathogen load (11,12). In contrast, mouse models of Mtb infection have shown that IM are more restrictive to bacterial growth as compared to AM (13,14).

Although BCG is typically administered intradermally, recent studies demonstrate that vaccination route significantly impacts protective immunity against Mtb. In non-human primates, intravenous

78 BCG vaccination conferred robust protection following Mtb challenge, induced markedly higher
79 frequencies of antigen-responsive CD4 and CD8 T cells in blood, lung parenchyma, and
80 bronchoalveolar lavage fluid compared to intradermal vaccination, and conferred robust protection
81 following Mtb challenge (15,16). Subsequent studies showed that high-dose IV BCG drives an
82 influx of polyfunctional T cells and recruited macrophages into airways, with both CD4+ and
83 CD8α+ T cells required for protection (15,17). Similar route dependent effects have been observed
84 in mice. Intranasal but not subcutaneous BCG vaccination activates AM, enhancing metabolic and
85 activation gene signatures and improving bacterial control after both Mtb and *Streptococcus*
86 *pneumoniae* challenge (18). More recently, IV BCG was shown to generate a CX3CR1-high CD4+
87 effector memory T cell subset capable of mediating cross protection against influenza via IFNγ
88 dependent activation of AM (19).
89
90 Collectively, these findings suggest that vaccination route shapes immune responses in the lung,
91 with protection strongly correlating with enhanced T cell and macrophage activation. However,
92 studies to date have focused primarily on AM while the impact on IM biology remains largely
93 unexplored. Notably, IM express high levels of the anti-microbial effector NOS2 during Mtb
94 infection in mice, suggesting a potential role in early bacterial control (14). Whether vaccination,
95 particularly via alternative routes, enhances IM antimicrobial capacity remains unknown. This gap
96 is especially relevant given growing interest in mucosal vaccination strategies which may directly
97 engage pulmonary macrophages at the site of pathogen entry and negate safety concerns associated
98 with IV BCG injection.
99
100 To directly compare how vaccine delivery route shapes lung macrophage biology, we immunized
101 mice with BCG via SC, IV, or mucosal IT administration. High-dimensional flow cytometry and
102 single-cell RNA sequencing (scRNA-Seq) revealed that IT vaccination selectively expands a
103 distinct IM subset enriched for metabolic, antimicrobial, and type I/II IFN-response programs that
104 were not observed after SC or IV delivery. Consistent with these findings, IT BCG elicited the
105 strongest protection in Mtb rechallenge experiments. Integration of cell-cell interaction analyses
106 and spatial transcriptomics uncovered potential IM - CD4 T cell interactions and demonstrated
107 that activated IM localize to distinct regions of the lung following IT BCG. Together, these
108 findings identify IM reprogramming as a previously underappreciated component of mucosal BCG

109 immunity and highlight mucosal vaccination as a promising strategy to harness lung macrophages
110 for improved protection against Mtb.

111 **Results.**

112 **IT BCG supports enhanced IM activation.**

113 Given that lung macrophages are among the first immune cells to encounter pulmonary Mtb, we
114 focused on how the route of BCG vaccination differentially rewired these cells. Wild type (WT)
115 mice were vaccinated with SC, IT, or IV BCG, and after 8 weeks lungs were harvested and
116 analyzed by high dimensional flow cytometry using a gating strategy designed to identify AM, IM
117 as well as other myeloid cells (Supplementary Fig. 1 A) (6).
118
119 The frequency of AM was reduced after IT and IV vaccination compared to naïve mice but the
120 absolute numbers remained unchanged (Fig. 1 A). Analysis of typical macrophage activation
121 markers including CD80, CD86 and MHCII revealed increased expression after IT and IV, but not
122 SC, vaccination in AM (Fig. 1 B). CD38 has recently been described as a marker of macrophages
123 which possess an enhanced ability to control Mtb (20). Following IT and IV vaccination the
124 frequency of CD38 positive AM was increased (Fig. 1 C). In contrast, SC BCG did not lead to
125 enhanced CD38 expression on AM (Fig. 1 C). The frequency of NOS2 positive AM increased by
126 a small but significant extent following IT and IV, but not SC, vaccination (Fig. 1 D). We next
127 examined the AM phenotype at an earlier time point of 4 weeks post vaccination. Following IT
128 and IV vaccination the expression of CD80, CD86 and MHCII was increased on AM, as was the
129 frequency of CD38 positive cells. Similar to the 8 week time point, SC BCG did not enhance the
130 expression of the analysed markers (Supplementary Fig. 1 B-D). At a later timepoint of 12 weeks
131 post vaccination the increased expression of CD86 and MHCII was maintained in IT and IV
132 vaccinated groups as compared to naive or SC vaccinated mice (Supplementary Fig. 1 E).
133 Increased frequencies of CD38 or NOS2 positive AM were only observed in the IT vaccinated
134 group (Supplementary Fig. 1 F, G).
135
136 Within the IM compartment we observed an increase in both cell frequency and absolute numbers
137 8 weeks after IT BCG (Fig. 1 E). Analysis of activation markers revealed increased expression of
138 CD80, no change in CD86 and downregulation of MHCII after IT and IV BCG (Fig. 1 F). In
139 contrast to AM, the frequency of CD38 positive IM increased after all routes of vaccination (Fig.

140 1 G), while NOS2 expression was significantly increased only after IT BCG (Fig. 1 H), suggesting
141 route-specific enhancement of antimicrobial effector capacity. At 4 weeks post vaccination CD80
142 expression was increased after IT and IV BCG, however CD86 and MHCII levels were decreased
143 (Supplementary Fig. 1 H). Furthermore, IT and IV BCG also increased the frequencies of both
144 CD38 and NOS2 positive cells (Supplementary Fig. 1 I, J). By 12 weeks post vaccination IM from
145 IT BCG mice maintained elevated CD80 expression, whereas the expression of the other analyzed
146 markers appeared to be returning to baseline (Supplementary Fig. 1 K-M). Together, these data
147 indicate that IT and IV BCG exert significant alterations to the phenotype of both AM and IM,
148 while SC BCG has a minimal impact.
149
150 Since viable BCG is present up to 12 weeks post IT and IV vaccination (Supplementary Fig. 1 N),
151 we next wondered if the continued presence of bacteria was required for driving the expression of
152 CD80, CD86 and MHCII by AM or IM. To examine this, cohorts of WT mice were vaccinated
153 using SC, IT or IV routes for a period of 8 weeks. Next, the animals were administered a cocktail
154 of antibiotics (rifampicin and isoniazid) in the drinking water for 4 weeks. Following a rest period
155 of 2 weeks, the lungs were harvested and analysed using flow cytometry. We observed similar
156 expression of CD80, CD86 and MHCII by AM after all routes of vaccination in antibiotic treated
157 and untreated mice (Supplementary Fig. 1 O). In the case of IM, antibiotic treatment did not
158 influence the expression of these markers, with the exception of increased MHCII expression in
159 IT-vaccinated mice (Supplementary Fig. 1 P).
160
161 We next used scRNA-Seq to more comprehensively characterize the transcriptional programs
162 underlying changes in macrophage phenotype. CD45 positive cells were sorted from the lungs of
163 naive mice as well as those that had been vaccinated with SC, IT or IV BCG 8 weeks prior. The
164 cell suspensions were stained with CITE-seq antibodies to facilitate the identification of the
165 various immune cell populations. We began our analysis by focusing on myeloid cells and using
166 surface markers and known marker genes, we identified AM, IM, DCs and monocytes (Fig. 2 A,
167 Supplementary Fig. 2 A-D). It was notable that among these populations SC BCG appeared to
168 have a minimal impact on the transcriptome of AM and IM (Supplementary Fig. 2 E). In contrast
169 IT and IV BCG resulted in alterations to the transcriptomic profile of both cell types
170 (Supplementary Fig. 2 F, G).

171 Pseudobulk differential expression analysis further revealed that IV BCG led to the most
172 upregulated genes in AM as compared to naïve controls (Supplementary Fig. 2 H), while IT BCG-
173 treated AM showed increased expression of antigen presentation genes *(H2-K1*, *H2-Ab1*) as well
174 as the chaperone protein *Cd74* (Supplementary Fig. 2 J). We next focused our analysis on IM after
175 vaccination and observed that IT BCG had the most profound effect in terms of the number of
176 upregulated genes (Fig. 2 B). Within these upregulated genes were a number of interferon targets
177 such as *Cxcl9*, *Gbp2, Stat1* and *Cd274* (Fig. 2 C). In addition, IM from IT BCG vaccinated mice
178 expressed several metabolic genes including *Gapdh*, *Nampt*, *Pkm*, *Fth1, Slc2a1* as well as *Acod1*
179 (Fig. 2 C). In line with this, gene set enrichment analysis revealed increased activity in pathways
180 associated with IFNγ response, OXPHOS and glycolysis in IM from IT vaccinated mice (Fig. 2
181 D). Given that the aforementioned analysis was performed on all IM, we wondered if only a subset
182 of IM were responsible for driving the expression of these pathways. We identified 6 clusters of
183 IM in naïve and vaccinated mice of which cluster 1 was present only after IT and IV vaccination
184 (Fig. 2 E, F). In order to examine if the IM within cluster 1 were the cells primarily activated
185 following BCG vaccination, we created a gene expression signature score (named activated IM)
186 based on the genes upregulated after IT BCG. This signature score was most highly expressed by
187 the IM present in cluster 1 (Fig. 2 G) indicating that this subset was primarily activated after IT
188 BCG.
189
190 **CD4 T cells likely produce IFNγ after all routes of BCG vaccination.**
191 Given that IM from IT vaccinated mice showed enrichment for IFNγ-response genes (Fig. 2 C-D),
192 we next sought to identify which immune cells were producing IFNγ. To do this we examined the
193 non-myeloid immune cells within our single cell data set and based on marker genes and surface
194 protein expression identified B cells, NK cells, as well as CD4 and CD8 T cells (Supplementary
195 Fig. 3 A, B). Within these lymphocyte populations *Ifng* expression was highest in the CD4 T cell
196 compartment (Supplementary Fig. 3 C). We therefore focused on examining route dependent
197 differences in CD4 T cells following BCG vaccination. 5 clusters of CD4 T cells were identified
198 in naïve and BCG vaccinated mice (Supplementary Fig. 3 D). Cluster 5 was present predominantly
199 in unvaccinated mice and were likely unactivated cells. Clusters 2 and 4 expressed genes such as
200 *Sell*, *Ccr7* and *S1pr1,* these are expressed by naïve and central memory CD4 T cells
201 (Supplementary Fig. 3 E, F). Despite sharing the expression of the above-mentioned genes, clusters

202 2 and 4 differed in their distribution among the experimental groups. Specifically, cluster 2 was
203 present only after IT and IV BCG while cluster 4 was present in SC vaccinated mice
204 (Supplementary Fig. 3 G). Genes higher in cluster 2 than cluster 4 suggest more active translational
205 machinery: *Eif3f* (a component of the translation initiation complex), the transcription factor *Klf13*,
206 *Chd3* (involved in chromatin remodeling), *Tut4* (involved in mRNA decay) and *Pnrc1*
207 (Supplementary Fig. 3 E, F).
208
209 Cluster 1 was present in all conditions but at a higher proportion in IT and IV vaccinated mice
210 (Supplementary Fig. 3 G). This cluster resembled migrating CD4 T cells (*Maf* and *Cxcr3*) and a
211 small proportion of Tfh cells (*Bcl6*, *Pdcd1*, *Izumo1r*, *Cxcr5*) (21). We next performed pseudobulk
212 differential expression analysis and compared how the CD4 T cells within cluster 1 differed after
213 each route of vaccination. After IT and IV vaccination, cells in cluster 1 had a higher expression
214 of both *Socs1* and *Jund* as compared to SC BCG, potentially indicating a more regulatory
215 phenotype (Fig. 3 A, B). In addition, *Tgfb* expression was increased after IT and IV as compared
216 to SC BCG. Beyond its role in tissue remodeling, TGFβ signaling has recently been described to
217 mediate the transition of monocytes to IM in the lung (10) and is required for AM survival (2,22).
218 Interestingly, when comparing cells within cluster 1 in the IT and IV groups, we observed
219 increased expression of *Hk2* in the IT group which may be indicative of enhanced metabolic
220 activity. These cells also exhibited higher expression of *Cxcr4* (a Tfh marker) and *Cxcr6* (a Th1
221 marker), genes which are involved in the homing to, and retention in, inflamed tissue (Fig. 3 C)
222 (23,24) .
223
224 CD4 T cells within cluster 3 expressed genes such as *Cx3cr1*, *Zeb2*, *Il18rap* and *Ifng*
225 (Supplementary Fig. 3 E, F). This cluster resembled a recently described effector memory subset
226 of CX3CR1^{hi} CD4 T cells that are induced following IV BCG (19). To confirm this apparent
227 similarity, we generated a gene expression signature score (named activated CD4 cells) based on
228 the aforementioned publication and overlaid it onto our single cell dataset. As expected, cluster 3
229 had the highest signature expression score followed by cluster 1 (Supplementary Fig. 3 H, I).
230 Notably, cluster 3 CD4 T cells were present at similar proportions across all vaccination routes
231 (Supplementary Fig. 3 G), prompting us to investigate whether functional differences might be
232 more apparent at the transcriptional level. When comparing IT and SC routes we observed that the

233 cells from the IT mice expressed metabolic genes such as *Glud1*, *Acadl*, *Coq2*, *Mff*, and *Tomm20*
234 suggesting an enhanced oxidative metabolism typical of memory cells. Moreover, they expressed
235 genes indicative of a regulatory profile like *Tgfb1, Ltb* and *Socs1* as well as the anti-apoptotic
236 genes *Mcl1* and *Bag1* (Fig. 3. D). In contrast, CD4 T cells within cluster 3 from SC BCG mice
237 appeared to be in a more inflammatory state. These cells expressed *Cd9* (a tetraspanin associated
238 with immune synapse formation), *Cxcl10* (involved in T cell recruitment), *Csf1* (indicating
239 ongoing communication with monocytes or macrophages) and *Tnfrsf4* (OX40, a costimulatory
240 receptor). Similar gene expression patterns were observed when cluster 3 CD4 T cells were
241 examined in the IV versus SC groups (Fig. 3 E).
242
243 To complement these data we performed additional flow cytometry experiments with a panel
244 targeting CD4 T lymphocytes (Supplementary Fig. 3 J). 8 weeks after vaccination the absolute cell
245 number of total CD4 T cells was increased in IT BCG mice (Supplementary Fig. 3 K, L). In
246 addition, the frequency and number of tissue resident CD45 IV negative CD4 T cells was increased
247 after IT BCG (Fig. 3 G-I). In line with this we observed an increase in the number of total CD4 T
248 cells expressing the residency marker CD69 (Fig. 3 J). Further, CD45 IV negative CD4 T cells
249 from IT BCG mice increased expression of CD44, CXCR3 and CXCR6, collectively indicating
250 enhanced activation and potential tissue retention (Fig. 3 K-M).
251
252 **IM-CD4 T cell crosstalk following BCG Vaccination.**
253 Having identified route specific differences in both IM and CD4 T cell phenotypes, we next
254 performed NicheNet analysis to understand if these cell types were directly interacting. For this
255 analysis we separated CD4 T cells from cluster 3 (labeled activated CD4 T cells) from the other
256 clusters (labeled as CD4 T cells). This confirmed that activated CD4 T cells were the primary
257 potential source of IFNγ for IM after all vaccination routes (Fig. 4 A-C) and that this was signaling
258 via *Ifngr1* and *Ifngr2* on IM (Supplementary Fig. 4 A-C). Next, we wondered if IM were
259 reciprocally signaling to CD4 T cells. NicheNet analysis predicted that after IT BCG, IM signal to
260 CD4 T cells primarily via the chemokines *Ccl3*, *Cxcl10* and *Cxcl16* (Fig. 4 E). *Cxcl16* was
261 predicted to signal via *Cxcr6* (Supplementary Fig. 4 E). The predicted *Cxcl16*/*Cxcr6* signaling axis
262 was consistent with our flow cytometry data showing increased CXCR6 expression on CD4 T cells
263 after IT vaccination (Fig. 3 N-P). IM from IV BCG mice were similarly providing *Ccl3* and *Cxcl16*

264 (Fig. 4 F). In contrast to IT and IV vaccination, CD4 T cells from SC BCG mice were not receiving
265 these ligands from IM and instead were receiving a distinct set of signals including *Il-1b,* as well
266 as *Ifng* from activated CD4 T cells (Fig. 4 D). Collectively these data suggest that mucosal IT
267 vaccination establishes a bidirectional IM-CD4 T cell circuit such that IM derived CXCL16
268 promotes the recruitment of CD4 T cells to the lung, which in turn provide IFNγ to sustain IM
269 activation.
270
271 **Activated IM localise in distinct tissue niches within the lung.**
272 Since NicheNet had indicated that IM and CD4 T cells may be potential interaction partners, we
273 decided to investigate if these cell types localized to distinct niches within the tissue using spatial
274 transcriptomics. Lung slices were taken 8 weeks after IV, IT or SC BCG, as well as from naïve
275 controls, and analyzed using the 10x Genomics Visium platform. Spatial clustering resulted in 21
276 clusters across the samples (Fig. 5 A, Supplementary Fig. 5 A). Of these, clusters 4, 18 and 19
277 were found predominately in IT and IV slices but not in SC BCG or naïve samples (Fig. 5 B, C,
278 Supplementary Fig. 5 B). To determine the cellular composition of these vaccination induced
279 clusters, we performed cell type deconvolution using RCTD based on our parallel single cell data.
280 This analysis returns weights that estimate the cell type proportions in each spot. Cluster 4 had a
281 bigger proportion of structural cells such as endothelial cells and fibroblasts while cluster 18 and
282 19 were enriched with immune cells. In particular cluster 18 had a higher proportion of activated
283 IM, B cells, T lymphocytes and other immune cells (Fig. 5 D).
284
285 To assess whether the activated immune cell populations identified in our scRNA-seq analysis
286 localized to IT/IV specific tissue regions we overlaid our activated IM gene expression signature
287 score onto the spatial slices. This signature was highly expressed in the regions occupied by spatial
288 clusters 18 and 19 in the slices taken from IT and IV vaccinated lungs (Fig. 5 E, Supplementary
289 Fig. 5 C). Similarly, B cell and activated CD4 T cell signatures showed strongest expression in
290 these same tissue regions, with the CD4 signature showing somewhat broader distribution across
291 the section (Fig. 5 F, G, Supplementary Fig. 5 D, E). Notably, expression of *Cxcl16* and *Cxcr6*
292 was also concentrated in these areas, consistent with our NicheNet predictions of IM-CD4 T cell
293 interactions (Supplementary Fig. 5 F). The co-localization of activated IM, B cells and CD4 T cells
294 suggest that these regions are likely inducible bronchus-associated lymphoid tissue (iBALT),

295 preferentially formed after IT and IV, but not SC, BCG vaccination. Whether proximity to iBALT
296 facilitates rewiring of lung macrophages following BCG vaccination is currently unclear and
297 warrants further investigation.
298
299 **IT BCG vaccination confers superior protection during Mtb challenge.**
300 To assess if the observed changes in IM phenotype and tissue localization following IT BCG
301 translated to superior protection we performed rechallenge experiments. WT mice were vaccinated
302 with BCG Pasteur via SC, IV, or IT routes. Sixty days later, vaccinated and unvaccinated mice
303 were challenged with fluorescent Mtb, and lung bacterial burden was measured 14 days post-
304 infection (Fig. 6 A). As compared to unvaccinated controls, mice that had received prior IT
305 vaccination exhibited the greatest reduction in Mtb burden (Fig. 6 B). Flow cytometric analysis
306 confirmed Mtb infection of neutrophils, DCs, AM, and IM, and revealed decreased Mtb signal in
307 these populations in all vaccinated groups (Fig. 6 C and Supplementary Fig. 6 A-D).
308
309 Next, we analyzed the expression of the anti-microbial effector molecule NOS2 across myeloid
310 populations. Among the analyzed cell types, DCs - but not neutrophils - expressed NOS2, and the
311 frequency of NOS2+ DCs increased following SC, but not IT or IV BCG (Fig. 6 D Supplementary
312 Fig. 6 E, F). Very few AM exhibited NOS2 expression in Mtb infected mice and was only slightly
313 enhanced by prior BCG vaccination (Fig. 6 D). Instead, robust NOS2 expression was observed in
314 IM following Mtb infection (Fig. 6 D and supplementary Fig. 6 H). Notably, IM from SC
315 vaccinated mice also expressed significant NOS2 levels after Mtb challenge, despite SC BCG
316 having minimal impact on IM phenotype. Given the higher bacterial burden in SC vaccinated mice,
317 this might reflect infection-driven rather than vaccine-induced NOS2.
318
319 To complement the above data and to more directly assess whether IT BCG enhanced IM effector
320 function in the absence of antigen-specific adaptive immunity, we next established an acute
321 infection model using the opportunistic pathogen *Pseudomonas aeruginosa* (PA). Cohorts of WT
322 mice were vaccinated for 8 weeks as described above and then challenged with PA. 24 hours after
323 infection bacterial burden in the lung was assessed via agar plating (Fig. 6 E). Mice that had
324 received prior IT and IV, but not SC, BCG had significantly reduced bacterial load as compared
325 to unvaccinated mice (Fig. 6F). Using flow cytometry, we observed that the frequency of IM

326 increased after infection and this was most pronounced in mice vaccinated with IT BCG (Fig. 6
327 G). Additionally, CCR2 expression was increased on IM across all vaccination routes, likely
328 indicative of monocyte influx following PA infection (Fig. 6H). Within CCR2- IM we observed
329 only minimal NOS2 production from unvaccinated mice infected with PA. Instead, these cells
330 expressed Arginase 1 (Arg1), a marker typically associated with the resolution stages of
331 inflammation (Fig. 6 I, J). PA-induced Arg1 expression may indicate that IM are being skewed
332 away from bacterial control and toward limiting tissue inflammation. Strikingly, prior IT BCG
333 vaccination significantly boosted NOS2 expression by IM while limiting Arg1 (Fig. 6 I, J).
334 Interestingly, we also observed an accumulation of NOS2+Arg1+ double positive IM in IT BCG
335 mice infected with PA (Fig. 6 I, J). NOS2 and Arg1 expression have traditionally been used as
336 markers of opposing macrophage polarization states, particularly in *in vitro* studies. The presence
337 of an IM population co-expressing both markers suggests macrophage heterogeneity or the
338 concurrent activation of multiple signaling pathways, underscoring the complexity of the
339 inflammatory tissue microenvironment. Collectively our data demonstrate that mucosal BCG
340 administration is protective against both homologous and heterologous bacterial pathogens and
341 point to IM as a central mediator of protection.
342
343 **Discussion.**
344 In this study we investigated how the route of BCG vaccination differentially programs pulmonary
345 macrophages and influences subsequent protection. Using high dimensional flow cytometry, we
346 observed that IT and IV BCG vaccination resulted in similar upregulation of surface and activation
347 markers in AM and IM, while macrophages from SC BCG mice more closely resembled naïve
348 cells. ScRNA-seq confirmed that SC BCG induced minimal changes in AM and IM. Notably, our
349 transcriptome data revealed that mucosal IT BCG predominantly rewired lung IM while exerting
350 a less pronounced effect on AM. IM from IT BCG vaccinated mice exhibited enhanced expression
351 of genes downstream of type I/II interferon signaling, as well as metabolic genes involved in
352 glycolysis and oxidative phosphorylation. Our antibiotic data suggest that this IM phenotype is
353 maintained without viable BCG, suggesting potential epigenetic rewiring following vaccination.
354 Future work will incorporate challenge experiments in antibiotic-treated, BCG vaccinated mice to
355 investigate this further.

356 Because IM functional capacity may depend on developmental origin, an unresolved question is
357 whether activated IM induced after IT BCG arise from recruited monocytes or from locally rewired
358 resident IM. This could be addressed by flow cytometric analysis of bone marrow to determine
359 whether mucosal BCG alters progenitor composition, combined with genetic fate mapping models
360 to define IM ontogeny. Consistent with systemic progenitor reprogramming, a non-human primate
361 (NHP) study found that mucosal BCG induces transcriptional and metabolic signatures of trained
362 immunity in blood and bone marrow monocytes (25).
363
364 Beyond IM reprogramming, our data further reveal spatially organized IM-CD4 T cell crosstalk
365 as a potential mechanism underlying mucosal vaccine efficiency. Our transcriptome data identified
366 CD4 T cells to be a source of IFNγ, and cell-cell communication analysis suggested reciprocal
367 signaling between IM and CD4 T cells following IT BCG. Mucosal vaccination led to the
368 enrichment of lung-resident CD4 T cells with increased expression of activation markers and
369 chemokine receptors. Spatial transcriptomics further indicated that activated IM localize in close
370 proximity to CD4 T cells within iBALT regions, raising the possibility that IT BCG establishes
371 immune niches that position CD4 T cells and IM for sustained, bidirectional signaling. A previous
372 study demonstrated that a subset of IM is required for iBALT formation in the lung during a house
373 dust mite model (8). However, whether proximity to iBALT is necessary to drive IM activation—
374 particularly during secondary infections—remains unclear. Conceptually, the iBALT niche may
375 facilitate IM–CD4 T-cell crosstalk or provide additional cytokine signals beyond IFNγ that
376 influence IM behavior. Experiments that disrupt iBALT formation, e.g. by using LTBR-Fc (26),
377 after BCG vaccination but prior to secondary infection may shed light on this issue.
378
379 These spatial findings raise the possibility that IM guide CD4 T cell localization to and/or within
380 the lung via CXCL16/CXCR6, which in turn facilitates IM activation via T cell derived IFNγ.
381 Supporting this idea, a recent study found CXCL16-positive macrophages situated in close
382 proximity to CXCR6-expressing T cells at the iBALT periphery following influenza infection (27).
383 Future work to assess cytokines in lung homogenates across multiple timepoints post vaccination,
384 as well as the effects of CXCL16 blockade and lymphocyte depletion, will help clarify the
385 mechanistic basis of IT BCG induced programming of IM and the requirement for CD4 T cells in
386 this process (28).

387

388 In our Mtb challenge model, mice vaccinated with IT BCG demonstrated the strongest protection
389 (i.e. had the lowest bacterial burden) compared to the other routes. This increased protective
390 capacity was not solely attributable to BCG presence in the lung, since IV mice had similar BCG
391 burdens at 4- and 8-weeks post vaccination. We propose that direct IT delivery to the lung
392 facilitates faster uptake of BCG by IM combined with earlier CD4 T cell recruitment, both of
393 which would enable IM epigenetic adaptation. A functional consequence of IM reprogramming is
394 further implied by our *P. aeruginosa* acute infection model, where IM from IT BCG vaccinated
395 mice expressed the highest levels of NOS2. This suggests that IT BCG licenses IM for rapid
396 activation after challenge, thereby facilitating early bacterial clearance. However, while our data
397 strongly implicate IM as key mediators of IT BCG induced protection, we cannot exclude a
398 contributory role for AM, particularly during early pathogen encounter. Future work using recently
399 developed IM-specific (8,9) and AM-specific (29) depletion models will definitively address the
400 relative contributions of each population during bacterial challenge.

401

402 Our findings strengthen the rationale for mucosal BCG as a vaccination strategy and complement
403 recent controlled human infection model studies evaluating the effects of route-specific BCG
404 vaccination in humans (30,31). However, our observation that SC and IV vaccinated mice
405 exhibited similar Mtb burdens appears to diverge from the findings of Darrah et al. (16) who
406 reported superior protection following IV BCG compared to intradermal administration in NHPs.
407 Several factors may contribute to this difference. First, the kinetics and magnitude of BCG induced
408 immunity may differ between mice and NHPs. Second, we assessed Mtb burden at 2 weeks post
409 challenge whereas Darrah et al. evaluated protection at 12 weeks; accordingly, it is possible that
410 IT and IV vaccination would both demonstrate superior protection relative to SC vaccination at
411 later time points in mice. Third, differences in BCG inoculum (1×10^6 in our study versus 5×10^7
412 in Darrah et al.) and/or the dose for Mtb challenge (100-200 CFU in our study versus 4-36 CFU in
413 Darrah et al.) may influence the magnitude of protection.
414 In summary, our study demonstrates that the route of BCG vaccination critically shapes pulmonary
415 macrophage reprogramming, with mucosal delivery uniquely licensing IM for enhanced activation
416 potentially through spatially organized immune interactions. These findings establish a

417 mechanistic framework for optimizing mucosal vaccination strategies against tuberculosis and
418 other respiratory pathogens.

419 **Methods**

420 **KEY RESOURCES TABLE**

REAGENT OR RESOURCE	SOURCE	IDENTIFIER
Antibodies		
CD11b BV510 (Clone M1/70)	Biolegend	Cat#101245, RRID:AB_2561390
IA/IE AlexaFluor700 (Clone M5/114.15.2)	Biolegend	Cat#107621, RRID:AB_493726
CD86 PE-Dazzle594 (Clone GL-1)	Biolegend	Cat#105041,RRID:AB_2566408
CD80 BV650 (Clone 16-10A1)	Biolegend	Cat#104731
F4/80 BV605 (Clone BM8)	Biolegend	Cat#123133, RRID: AB_2562305
CCR2 BV421 (Clone SA203G11)	Biolegend	Cat#150605, RRID:AB_2571913
CD64 BV711 (Clone X54-5/7.1)	Biolegend	Cat#139311, RRID:AB_2563846
CD11c BUV395 (Clone HL3)	BD Bioscience	Cat#564080, RRID:AB_2738580.
SiglecF BUV737 (Clone 1RNM44N)	BD Bioscience	Cat# 1RNM44N
CD11a/LFA1 FITC (Clone M17/4)	Biolegend	Cat#101106, RRID: AB_312779
MerTK PE (Clone 2B10C42)	Biolegend	Cat#151505, RRID:AB_2617036
CD45 APC-Fire810 (Clone 30-F11)	Biolegend	Cat103173, RRID:AB_2860599

CD45 Spark NIR 685 (Clone30-F11)	Biolegend	Cat#103168
CD45 Spark Blue 550 (Clone 30-F11)	Biolegend	Cat#103165
CD3 APC (Clone145-2C11)	Biolegend	Cat#100235, RRID:AB_2561455
NKp46 APC (Clone 29A1.4)	Biolegend	Cat#37607, RRID:AB_10612749
CD19 APC (Clone 6D5)	Biolegend	Cat#115512, RRID:AB_313647
iNOS Alexa Fluor 488 (CloneCXNFT)	eBioscience	Cat#53592082
Arg1 eFluor450 (Clone A1EXF5)	eBioscience	Cat#48369780
Lyve1 eFluor450 (Clone ALY7)	eBioscience	Cat#48044380
CD9 PECy7 (Clone MZ3)	Biolegend	Cat#124816
Ly-6G PerCP (Clone 1A8)	Biolegend	Cat#127653
Ly-6C APC Cy7 (Clone HK1.4)	Biolegend	Cat#128025
CD206 Alexa Fluor 647 (Clone C068C2)	Biolegend	Cat#141711
CD169 PerCp Cy5.5 (Clone 3D6.112)	Biolegend	Cat#142409
CX3CR1 BV785 (Clone SA011F11)	Biolegend	Cat#149029
TotalSeq B0301	Biolegend	Cat#155831
TotalSeq B0302	Biolegend	Cat#155833, RRID:AB_2814068
TotalSeq B0303	Biolegend	Cat#155835, RRID:AB_2814069
TotalSeq B0304	Biolegend	Cat#55837, RRID:AB_2814070

TotalSeq B0002 anti-mouse CD8a (Clone 53-6.7)	Biolegend	Cat#100783
TotalSeq B0001 anti-mouse CD4 (Clone RM4-5)	Biolegend	Cat#100573
TotalSeq B0431 anti-mouse CD170 (Clone S17007L)	Biolegend	Cat#155517
TotalSeq B0106 anti-mouse CD11c (Clone N418)	Biolegend	Cat#117359
TotalSeq B0202 anti-mouse CD64 (Clone X54-5/7.1)	Biolegend	Cat#139329
TotalSeq B0813 anti-mouse CD9 (Clone MZ3)	Biolegend	Cat#124823
Bacterial and virus strains		
PAO1 Wild-type *Pseudomonas aeruginosa*	U. Jenal, Biozentrum Basel	ID-UJP505 (32)
PAO1 *CTX::mCherry* chromosomal integration for constitutive expression of mCherry by the pX2 promoter.	U. Jenal, Biozentrum Basel	ID- UJP3715
M. tuberculosis HN878:Turbo635		
M. tuberculosis HN878		
BCG Pasteur	N. Aguiló, University of Zaragoza	N/A
BCG::symc'::mCherry		
BCG:GFP (Pasteur)	N. Aguiló, University of Zaragoza	(18)

Chemicals, peptides, and recombinant proteins		
DAPI	Merk	Cat#D9542-1MG
Liberase TL	Merk	Cat#5401020001
Liberase TM	Merk	Cat#5401119001
DNAse-I	Merk	Cat#10104159001
Collagenase P	Merck	Cat#11213857001
Dispase II	Merck	Cat#D4693
AccuCheck Counting Beads	Invitrogen	Cat#PCB100
Critical commercial assays		
Chromium Next GEM Single Cell 3' Kit v3.1	10x Genomics	Cat#1000269
3' Feature Barcode Kit	10x Genomics	Cat#1000262
Dual Index Kit NT Set A	10x Genomics	Cat#1000242
Chromium Next GEM Chip G Single Cell Kit	10x Genomics	Cat#1000120
Library Construction Kit	10x Genomics	Cat#1000190
Visium Gene Expression Slide and Reagent Kit	10x Genomics	Cat#1000184
Illumina Novaseq 6000	Illumina	Cat#1000724
Deposited data		
Datasets are available at GEO accession GSE319571 (scRNA-Seq) and GSE319572 (Spatial Transcriptomics)		
Experimental models: Organisms/strains		

Mouse: C57BL/6Rj	Jackson Laboratories	RRID:IMSR_JAX:000664
Software and algorithms		
FlowJo	BD Bioscience	https://www.flowjo.com/solutions/flowjo
GraphPad Prism	GraphPad	https://www.graphpad.com/
STARsolo (>=2.7.10a)		
Bioconductor R packages (see below)	N/A	https://bioconductor.org/
DropletUtils (1.24.0)		
scuttle (1.14.0)		
scater (1.32.1)		
bluster (1.14.0)		
singleR (1.32.0)		
limma(3.60.6)		
NicheNet (2.2.0)		
UCell (2.8.0)		
BayesSpace (1.14.0)		
spacexr (2.2.1)		
Gene sets: MsigDB mouse gene sets		https://www.gsea-msigdb.org/gsea/msigdb/index.jsp
Other		
N/A	N/A	N/A

421

422 **Animals.**

423 C57BL/6Rj (CD45.2) were purchased from Charles River. Mice in each experiment were 6-8
424 weeks old, same-sex littermates, maintained and bred in the specific pathogen–free animal facility
425 at the University of Basel. All animal experiments were performed in accordance with local and
426 Swiss federal guidelines.

427 **Bacterial culture.**

428 *M. bovis* BCG::symc'::mCherry (hereafter BCG::mCherry) was generated in the laboratory by
429 transformation with the pCHERRY3 plasmid (a kind gift from D. Russell, Cornell University).
430 BCG::mCherry*, M. bovis* BCG Pasteur and BCG:GFP (kindly gifted by N. Aguiló University of
431 Zaragoza) were grown in 7H9 broth (BD) 10% OADC (BD), 0.2% (v/v) glycerol and 0.05% (v/v)
432 Tween 80 (Sigma) under constant shaking at 37° C. After 2 to 4 days the preculture was then
433 diluted 1:100 in 7H9 media without Tween80. When bacteria reached an optical density (OD_{600})
434 of 0.8 to 1, bacteria were collected and washed with PBS (Sigma, D8662). Subsequently bacteria
435 was de-clumped by manual shaking with glass beads and the upper phase containing the single
436 cell suspension was collected. De-clumped bacterial cultures were frozen in 25% glycerol at -80°C
437 until further use. For colony-forming unit (CFU) determination bacterial suspension was plated on
438 7H11 agar plates.
439
440 HN878:turbo635 was generated in house by transformation with the plasmid pCHARGE3 kindly
441 gifted by Tanya Parish (33) (Addgene plasmid # 24658; http://n2t.net/addgene:24658;
442 RRID:Addgene_24658). HN878:turbo635 was grown in 7H9 broth (BD) 10% OADC (BD), 0.2%
443 (v/v) Glycerol, 0.1 mM sodium propionate and 50 mg/ml Hygromycin B (Roth) . Bacteria were
444 de-clumped by vortex shaking with glass beads and the upper phase containing the single cell
445 suspension was harvested and frozen at -80°C until use.
446
447 *P. aeruginosa* (PAO1, PAO1 CTX::mCherry) was kindly provided by U. Jenal, University of
448 Basel. *P. aeruginosa* was cultured in liquid LB and subsequently frozen in 70% glycerol. Prior to
449 infection *P. aeruginosa* was plated from frozen glycerol stock overnight at 37°C on LB agar plates.
450 Single colonies were picked and grown overnight at 37°C under constant shaking (170 rpm).
451 Overnight cultures were then diluted and collected at log phase (OD600 = 0.5).
452

453 ***Mtb* infection.**

454 Prior to aerolization, Mtb was declumped with a 27G metal tip. Mice were infected in an Aero3G
455 Third Generation Aerosolizer (Biaera). Stocks were titrated to result in a day 1 bacterial load of
456 approximately 100 CFU.

457

458 **BCG vaccination / *P. aeruginosa* infection.**

459 For intratracheal administration mice were anesthetized with vaporized isoflurane and than
460 infected intratracheally with $1x10^6$ CFU diluted in 50 µL of PBS (Gibco). For subcutaneous
461 injection $1x10^6$ CFU was delivered in 200 µL, while intravenous BCG ($1x10^6$ CFU) was
462 administered in 100 µL PBS.

463

464 **CFU plating.**

465 ***Mtb***: For determination of CFU the left lobe was mechanically homogenized in 1 mL of PBS-
466 Tween (0.05%) using soft tissue homogenizing CK28 prep tubes (Bertin technologies) in a
467 Precellys Evolution Touch homogenizer (Bertin technologies). Homogenates were then serially
468 diluted and plated on 7H11 agar plates containing 10% OADC, 0.2% (v/v) Glycerol, 50 mg/ml
469 Hygromycin B and 1 vial of MGIT PANTA™ Antibiotic mixture (BD). CFU were counted after
470 a 3 week incubation at 37°C.

471 ***P. aeruginosa*:** For determination of CFU lung lobes were digested as described above. 50 uL of
472 digest were removed prior to filtration and a serial dilution was plated on tetracycline selective LB
473 agar plates. CFU were counted after overnight incubation at 37°C.

474

475 **Tissue preparation.**

476 In some experiments, prior to euthanasia mice were anesthetized with vaporized isoflurane and a
477 CD45 (Spark Nir 685) antibody was administered intratracheally. After 20 minutes mice were
478 injected with CD45 (APC-Fire 810) intravenously and sacrificed after 5 minutes.

479 For isolation of macrophages or lymphocytes, lungs were harvested, minced with scissors and
480 digested with a digestion mix containing liberase TM or liberase TL (500 µg/ml, Roche) for 30
481 minutes at 37° C under constant shaking. Single cell suspensions were generated by repeated
482 pipetting and filtering through 70 µm cell strainers (Milteny Biotec) in HBSS buffer (Hanks'
483 Balanced Salt solution, Sigma, H6648-500mL, 0.2% BSA and 0.5 mM EDTA). Erythrocytes were

484 lysed by addition of erythrocyte lysis buffer and the remaining lung cells were washed with HBSS
485 buffer.
486

487 **Single cell sequencing.**

488 For isolation of lymphocytes lungs were collected and diced into gentleMACS C Tubes (Miltenyi
489 Biotec) and washed down with 3 ml of media (RPMI, 10 mM aminoguanidine hydrochloride
490 (Sigma-Aldrich), 10 mM Hepes, penicillin-streptomycin-glutamine (100×, Gibco)), prewarmed in
491 a 37° C water bath. Digestion mix containing liberase TL (for lymphoid cells) (33.3 µg/ml, Merk)
492 and deoxyribonuclease I (58 µg/ml; Applichem) was added. Lungs were dissociated on a
493 gentleMACS Dissociator (Miltenyi Biotec) and mashed through 70 µm MACS SmartStrainers
494 (Miltenyi Biotec) as previously described (34). The isolation of stromal cells and myeloid cells
495 lungs has previously been described (35). In short: lobes were minced with scissors and digested
496 with 1mL of RPMI-1640 containing 0.8 mg/ml DispaseII and 0.2 mg/ml Collagenase P (both from
497 Roche), and 0.1 mg/ml DNase I (Invitrogen) at 37° C on a heating block and gently inverted and
498 mixed using a 1mL pipette every 5 min. After 15 min large fragments were spun down (10s) and
499 the supernatant was removed and filtered through a 70 µm MACS SmartStrainer into a tube
500 containing 5mL of Lung Media ((RPMI, 10 mM aminoguanidine hydrochloride (Sigma-Aldrich),
501 10 mM HEPES, penicillin-streptomycin-glutamine (100x, Gibco), 2% FCS, 0.5mM EDTA)).
502 Another 1mL of digestion mix was added to the remaining lung fragments and the process was
503 repeated two more times. Finally, erythrocytes were lysed by addition of ELB (155mM NH4Cl,
504 170mM tris-HCL), remaining cells were washed with FACS buffer (PBS, 2% FCS, and 0.1%
505 sodium azide) and further processed for sorting and subsequent single cell sequencing.
506

507 **Flow cytometry staining.**

508 For all fluorochrome-conjugated antibody dilutions, FACS buffer containing Fc block (Clone
509 2.4G2 InVivoMAb anti-mouse CD16/CD32; BioXCell, #BE0307) was used. Live-dead stain
510 (Zombie Fixable Viability™ Sampler Kit; BioLegend) was added to the antibody mix and stained
511 at RT 10 min. FoxP3 Transcription Factor Staining Buffer Set (eBioscience) was used for
512 intracellular staining. Flow cytometric analysis was performed on Cytek Aurora. Data was
513 analyzed using FlowJo X software (BD) and SpectroFlo (Cytek). Absolute cell numbers were

514 determined using AccuCheck Counting Beads (Invitrogen) based on the manufacturer
515 instructions.
516
517 **Single cell RNA sequencing.**
518 Lungs of naïve or BCG infected mice were removed and processed as described above for isolation
519 of lymphocytes or stromal/myeloid cells. Individual mice were hash tagged using TotalSeq-B anti-
520 mouse hashtag antibodies (B0301-B0304, BioLegend) and TotalSeq-B CITE-seq antibodies
521 (lymphocytes: CD8a (B0002), CD4 (B0001); myeloid cells: SiglecF (B0431), CD11c (B0106),
522 CD64 (B0202), CD9 (B0813)). Live, CD45+ and CD45- cells were sorted from lungs at 80 d.p.i.
523 and submitted for library preparation. A total of 10,000 target cells per sample were loaded. Single-
524 cell capture and cDNA library preparation was performed according to manufacturer's instructions
525 using 10x Genomics Chromium Next GEM Single Cell 3' Kit v2 reagents using dual indexing.
526 Sequencing was carried out on an Illumina Novaseq 6000 at the Genomics Facility Basel, ETH
527 Zurich.
528
529 Raw reads were mapped to the *Mus musculus* reference mm10_ensdb102 using STARsolo (36),
530 and empty droplets were removed with DropletUtils (37,38). The four replicate samples were
531 demultiplexed using hashtag oligos (HTO). Cells were filtered for library size, library complexity,
532 and mitochondrial content using adaptive thresholding implemented in the *perCellQCFilters*
533 function from the R package scuttle with default arguments (39). PCA and UMAP on the PCA-
534 reduced dimensions, were performed using the R package scater (39). Cells were clustered either
535 hierarchically using Ward's method or with the graph-based Leiden method using the bluster R
536 package. Cell annotation was performed with SingleR (40), and pseudo-bulk differential
537 expression analysis was conducted using the *pseudoBulkDGE* function from the scran R package
538 (1.32.0), following the Bioconductor OSCA book
539 (https://bioconductor.org/books/release/OSCA/). Lists of differentially expressed genes per cell
540 type and BCG route comparison are available in Supplementary Table 1. Gene set enrichment
541 analysis was performed using camera (41) from the limma R package (42) with MSigDB mouse
542 gene sets. Cell-cell interactions were interrogated using NicheNet (43) following the step-by-step
543 vignette starting from a Seurat object. When possible, lists of differentially expressed genes

544 derived from the pseudo-bulk differential expression analysis were provided to NicheNet for
545 comparison across cell types. Gene signature scores were calculated using UCell (44).
546
547 **Visium Spatial gene expression.**
548 Lungs were inflated with a 1:1 mixture of Tissue-Tek® O.C.T. Compound (Sakura) and PBS and
549 embedded in O.C.T. Tissues were sectioned at 10 µm on a cryostat. Further processing and
550 placement of sections was performed according to the protocol CG000240 (10X Genomics).
551 Following sample placement, sections were stained with DAPI according to the protocol
552 CG000312 (10X Genomics) and imaged using a Leica DMI 4000/6000 Widefield Microscope.
553 Sections were then permeabilized and prepared for library preparation according to the protocol
554 CG000239 (10X Genomics). Sequencing was carried out on an Illumina Novaseq 6000 at the
555 Genomics Facility Basel, ETH Zurich.
556
557 The fiducial frame of the Visium slides was aligned using Loupe Browser, and the resulting JSON
558 file was provided to Space Ranger to obtain count matrices. Spots outside the tissue, with library
559 size < 2000, or with mitochondrial content > 10% were filtered out. Spatial clustering was
560 performed using BayesSpace after joining spatial coordinates across samples and integrating
561 transcriptomic data, enabling spatial clusters to be shared between samples (45). The single-cell
562 dataset was used as a reference for deconvolution with RCTD from the spacexr R package (46).
563 Signature scoring and plotting were performed as for single-cell data using Bioconductor 3.19.
564
565 **Quantification and statistical analysis.**
566 Prism software (GraphPad 10. 4.1) was used for all statistical analyses. Unless otherwise stated
567 One-Way ANOVA with Tukey's multiple comparison test was used to determine statistical
568 significance. Statistical significances are indicated by *p<0.05, **p<0.005, ***p<0.0005,
569 ****p<0.0001, ns, not significant (p > 0.05). In summary graphs, points indicate individual
570 samples. All error bars are mean with SEM.
571
572 **Acknowledgements.**
573 We are indebted to Gaël Auray and all members of the University of Basel flow cytometry core
574 facilities for cell sorting and troubleshooting, furthermore we thank all staff at the BSL2 and BSL3

575 animal facilities of the University of Basel. In addition we are grateful to the University of Basel
576 Genomics Core. Bioinformatic calculations were performed at sciCORE (http://scicore.unibas.ch/)
577 scientific computing center at University of Basel. We thank all members of the King laboratory
578 for productive and helpful discussion. This work was supported by the Swiss National Science
579 Foundation, grant 212344 awarded to CGK, the State Secretariat for Education, Research and
580 Innovation (SERI), grant REF-1131.52304 awarded to CGK and the University of Basel Research
581 Fund for Junior Researchers awarded to AJF. The authors have no conflicting financial interests.
582

583 **Competing Interests.**

584 All authors declare no conflict of interest in relation to this manuscript.

585 **References.**

586 1. Global tuberculosis report 2025 [Internet]. World Health Organization; Available
587 from: https://www.who.int/teams/global-programme-on-tuberculosis-and-lung-
588 health/tb-reports/global-tuberculosis-report-2025

589 2. Aegerter H, Lambrecht BN, Jakubzick CV. Biology of lung macrophages in health
590 and disease. Immunity. 2022 Sep;55(9):1564–80.

591 3. Jeyanathan M, Vaseghi-Shanjani M, Afkhami S, Grondin JA, Kang A, D'Agostino
592 MR, et al. Parenteral BCG vaccine induces lung-resident memory macrophages and
593 trained immunity via the gut–lung axis. Nat Immunol. 2022 Dec;23(12):1687–702.

594 4. Russell DG, Simwela NV, Mattila JT, Flynn J, Mwandumba HC, Pisu D. How
595 macrophage heterogeneity affects tuberculosis disease and therapy. Nat Rev
596 Immunol. 2025 May;25(5):370–84.

597 5. Chakarov S, Lim HY, Tan L, Lim SY, See P, Lum J, et al. Two distinct interstitial
598 macrophage populations coexist across tissues in specific subtissular niches.
599 Science. 2019 Mar 15;363(6432):eaau0964.

600 6. Gibbings SL, Thomas SM, Atif SM, McCubbrey AL, Desch AN, Danhorn T, et al.
601 Three Unique Interstitial Macrophages in the Murine Lung at Steady State. Am J
602 Respir Cell Mol Biol. 2017 Jul;57(1):66–76.

603 7. Ural BB, Yeung ST, Damani-Yokota P, Devlin JC, De Vries M, Vera-Licona P, et
604 al. Identification of a nerve-associated, lung-resident interstitial macrophage subset
605 with distinct localization and immunoregulatory properties. Sci Immunol. 2020 Mar
606 13;5(45):eaax8756.

607 8. Li X, Mara AB, Musial SC, Kolling FW, Gibbings SL, Gerebtsov N, et al.
608 Coordinated chemokine expression defines macrophage subsets across tissues. Nat
609 Immunol. 2024 Jun;25(6):1110–22.

610 9. Vanneste D, Bai Q, Hasan S, Peng W, Pirottin D, Schyns J, et al. MafB-restricted
611 local monocyte proliferation precedes lung interstitial macrophage differentiation. Nat
612 Immunol. 2023 May;24(5):827–40.

613 10.Peng W, Vanneste D, Bejarano D, Abinet J, Meunier M, Radermecker C, et al.
614 Endothelial-driven TGFβ signaling supports lung interstitial macrophage development
615 from monocytes. Sci Immunol. 2025;

616 11.Strickland AB, Chen Y, Sun D, Shi M. Alternatively activated lung alveolar and
617 interstitial macrophages promote fungal growth. iScience. 2023 May;26(5):106717.

618 12.Dumigan A, Cappa O, Morris B, Sá Pessoa J, Calderon-Gonzalez R, Mills G, et al.
619 *In vivo* single-cell transcriptomics reveal *Klebsiella pneumoniae* skews lung
620 macrophages to promote infection. EMBO Mol Med. 2022 Dec 7;14(12):e16888.

621 13.Cohen SB, Gern BH, Delahaye JL, Adams KN, Plumlee CR, Winkler JK, et al.
622 Alveolar Macrophages Provide an Early Mycobacterium tuberculosis Niche and
623 Initiate Dissemination. Cell Host Microbe. 2018 Sep;24(3):439-446.e4.

624 14.Pisu D, Huang L, Narang V, Theriault M, Lê-Bury G, Lee B, et al. Single cell
625 analysis of *M. tuberculosis* phenotype and macrophage lineages in the infected lung.
626 J Exp Med. 2021 Sep 6;218(9):e20210615.

627 15.Simonson AW, Zeppa JJ, Bucsan AN, Chao MC, Pokkali S, Hopkins F, et al.
628 Intravenous BCG-mediated protection against tuberculosis requires CD4+ T cells and
629 CD8α+ lymphocytes. J Exp Med. 2025 Apr 7;222(4):e20241571.

630 16.Darrah PA, Zeppa JJ, Maiello P, Hackney JA, Wadsworth MH, Hughes TK, et al.
631 Prevention of tuberculosis in macaques after intravenous BCG immunization. Nature.
632 2020 Jan 2;577(7788):95–102.

633 17.Peters JM, Irvine EB, Makatsa MS, Rosenberg JM, Wadsworth MH, Hughes TK,
634 et al. High-dose intravenous BCG vaccination induces enhanced immune signaling in
635 the airways. Sci Adv. 2025 Jan 3;11(1):eadq8229.

636 18.Mata E, Tarancon R, Guerrero C, Moreo E, Moreau F, Uranga S, et al. Pulmonary
637 BCG induces lung-resident macrophage activation and confers long-term protection
638 against tuberculosis. Sci Immunol. 2021 Sep 24;6(63):eabc2934.

639 19.Tran KA, Pernet E, Sadeghi M, Downey J, Chronopoulos J, Lapshina E, et al. BCG
640 immunization induces CX3CR1hi effector memory T cells to provide cross-protection
641 via IFN-γ-mediated trained immunity. Nat Immunol. 2024 Mar;25(3):418–31.

642 20.Pisu D, Johnston L, Mattila JT, Russell DG. The frequency of CD38+ alveolar
643 macrophages correlates with early control of M. tuberculosis in the murine lung. Nat
644 Commun. 2024 Oct 2;15(1):8522.

645 21.Kohlmeier JE, Cookenham T, Miller SC, Roberts AD, Christensen JP, Thomsen
646 AR, et al. CXCR3 Directs Antigen-Specific Effector CD4+ T Cell Migration to the Lung
647 During Parainfluenza Virus Infection. J Immunol. 2009 Oct 1;183(7):4378–84.

648 22.Bain CC, MacDonald AS. The impact of the lung environment on macrophage
649 development, activation and function: diversity in the face of adversity. Mucosal
650 Immunol. 2022 Feb;15(2):223–34.

651 23.Swarnalekha N, Schreiner D, Litzler LC, Iftikhar S, Kirchmeier D, Künzli M, et al. T
652 resident helper cells promote humoral responses in the lung. Sci Immunol. 2021 Jan
653 8;6(55):eabb6808.

654 24.Crotty S. T Follicular Helper Cell Biology: A Decade of Discovery and Diseases.
655 Immunity. 2019 May;50(5):1132–48.

656 25.Vierboom MPM, Dijkman K, Sombroek CC, Hofman SO, Boot C, Vervenne RAW,
657 et al. Stronger induction of trained immunity by mucosal BCG or MTBVAC vaccination
658 compared to standard intradermal vaccination. Cell Rep Med. 2021 Jan;2(1):100185.

659 26.Conlon TM, John-Schuster G, Heide D, Pfister D, Lehmann M, Hu Y, et al.
660 Inhibition of LTβR signalling activates WNT-induced regeneration in lung. Nature.
661 2020 Dec 3;588(7836):151–6.

662 27.de Lima J, Swarnalekha N, Bartoszek E, Litzler LC, Depew CE, Esposito M, et al.
663 HIF-1α+ CD4 T cells coordinate a tissue resident immune cell network in the lung.

664 28.Kastner AL, Marx AF, Dimitrova M, Abreu-Mota T, Ertuna YI, Bonilla WV, et al.
665 Durable lymphocyte subset elimination upon a single dose of AAV-delivered depletion
666 antibody dissects immune control of chronic viral infection. Immunity. 2025
667 Feb;58(2):481-498.e10.

668 29.Verwaerde S, Hastir JF, Schetters STT, Smole U, Seys L, Baptista AP, et al. Innate
669 type 2 lymphocytes trigger an inflammatory switch in alveolar macrophages.
670 Immunity. 2026 Jan;59(1):60-78.e9.

671 30.Davids M, Pooran A, Hermann C, Mottay L, Thompson F, Cardenas J, et al. A
672 Human Lung Challenge Model to Evaluate the Safety and Immunogenicity of PPD
673 and Live Bacillus Calmette-Guérin. Am J Respir Crit Care Med. 2020 May
674 15;201(10):1277–91.

675 31.Marshall JL, Satti I, Surakhy M, Harris SA, Morrison H, Wittenberg RE, et al. Early
676 mucosal responses following a randomised controlled human inhaled infection with
677 attenuated Mycobacterium bovis BCG. Nat Commun. 2025 May 29;16(1):4989.

678 32.Malone JG, Jaeger T, Spangler C, Ritz D, Spang A, Arrieumerlou C, et al. YfiBNR
679 Mediates Cyclic di-GMP Dependent Small Colony Variant Formation and Persistence
680 in Pseudomonas aeruginosa. Roy CR, editor. PLoS Pathog. 2010 Mar
681 12;6(3):e1000804.

682 33.Carroll P, Schreuder LJ, Muwanguzi-Karugaba J, Wiles S, Robertson BD, Ripoll J,
683 et al. Sensitive Detection of Gene Expression in Mycobacteria under Replicating and
684 Non-Replicating Conditions Using Optimized Far-Red Reporters. Neyrolles O, editor.
685 PLoS ONE. 2010 Mar 23;5(3):e9823.

686 34.Swarnalekha N, Schreiner D, Litzler LC, Iftikhar S, Kirchmeier D, Künzli M, et al. T
687 resident helper cells promote humoral responses in the lung. Sci Immunol. 2021 Jan
688 8;6(55):eabb6808.

689 35.Fletcher AL, Malhotra D, Acton SE, Lukacs-Kornek V, Bellemare-Pelletier A, Curry
690 M, et al. Reproducible Isolation of Lymph Node Stromal Cells Reveals Site-Dependent
691 Differences in Fibroblastic Reticular Cells. Front Immunol [Internet]. 2011 [cited 2026
692 Jan 30];2. Available from:
693 http://journal.frontiersin.org/article/10.3389/fimmu.2011.00035/abstract

36.Kaminow B, Yunusov D, Dobin A. STARsolo: accurate, fast and versatile mapping/quantification of single-cell and single-nucleus RNA-seq data [Internet]. Bioinformatics; 2021 [cited 2026 Jan 30]. Available from: http://biorxiv.org/lookup/doi/10.1101/2021.05.05.442755

37.participants in the 1st Human Cell Atlas Jamboree, Lun ATL, Riesenfeld S, Andrews T, Dao TP, Gomes T, et al. EmptyDrops: distinguishing cells from empty droplets in droplet-based single-cell RNA sequencing data. Genome Biol. 2019 Dec;20(1):63.

38.Griffiths JA, Richard AC, Bach K, Lun ATL, Marioni JC. Detection and removal of barcode swapping in single-cell RNA-seq data. Nat Commun. 2018 Jul 10;9(1):2667.

39.McCarthy DJ, Campbell KR, Lun ATL, Wills QF. Scater: pre-processing, quality control, normalization and visualization of single-cell RNA-seq data in R. Hofacker I, editor. Bioinformatics. 2017 Apr 15;33(8):1179–86.

40.Aran D, Looney AP, Liu L, Wu E, Fong V, Hsu A, et al. Reference-based analysis of lung single-cell sequencing reveals a transitional profibrotic macrophage. Nat Immunol. 2019 Feb;20(2):163–72.

41.Wu D, Smyth GK. Camera: a competitive gene set test accounting for inter-gene correlation. Nucleic Acids Res. 2012 Sep 1;40(17):e133–e133.

42.Ritchie ME, Phipson B, Wu D, Hu Y, Law CW, Shi W, et al. limma powers differential expression analyses for RNA-sequencing and microarray studies. Nucleic Acids Res. 2015 Apr 20;43(7):e47–e47.

43.Browaeys R, Saelens W, Saeys Y. NicheNet: modeling intercellular communication by linking ligands to target genes. Nat Methods. 2020 Feb 2;17(2):159–62.

44.Andreatta M, Carmona SJ. UCell: Robust and scalable single-cell gene signature scoring. Comput Struct Biotechnol J. 2021;19:3796–8.

45.Zhao E, Stone MR, Ren X, Guenthoer J, Smythe KS, Pulliam T, et al. Spatial transcriptomics at subspot resolution with BayesSpace. Nat Biotechnol. 2021 Nov;39(11):1375–84.

46.Cable DM, Murray E, Zou LS, Goeva A, Macosko EZ, Chen F, et al. Robust decomposition of cell type mixtures in spatial transcriptomics. Nat Biotechnol. 2022 Apr;40(4):517–26.

729

Figure 1

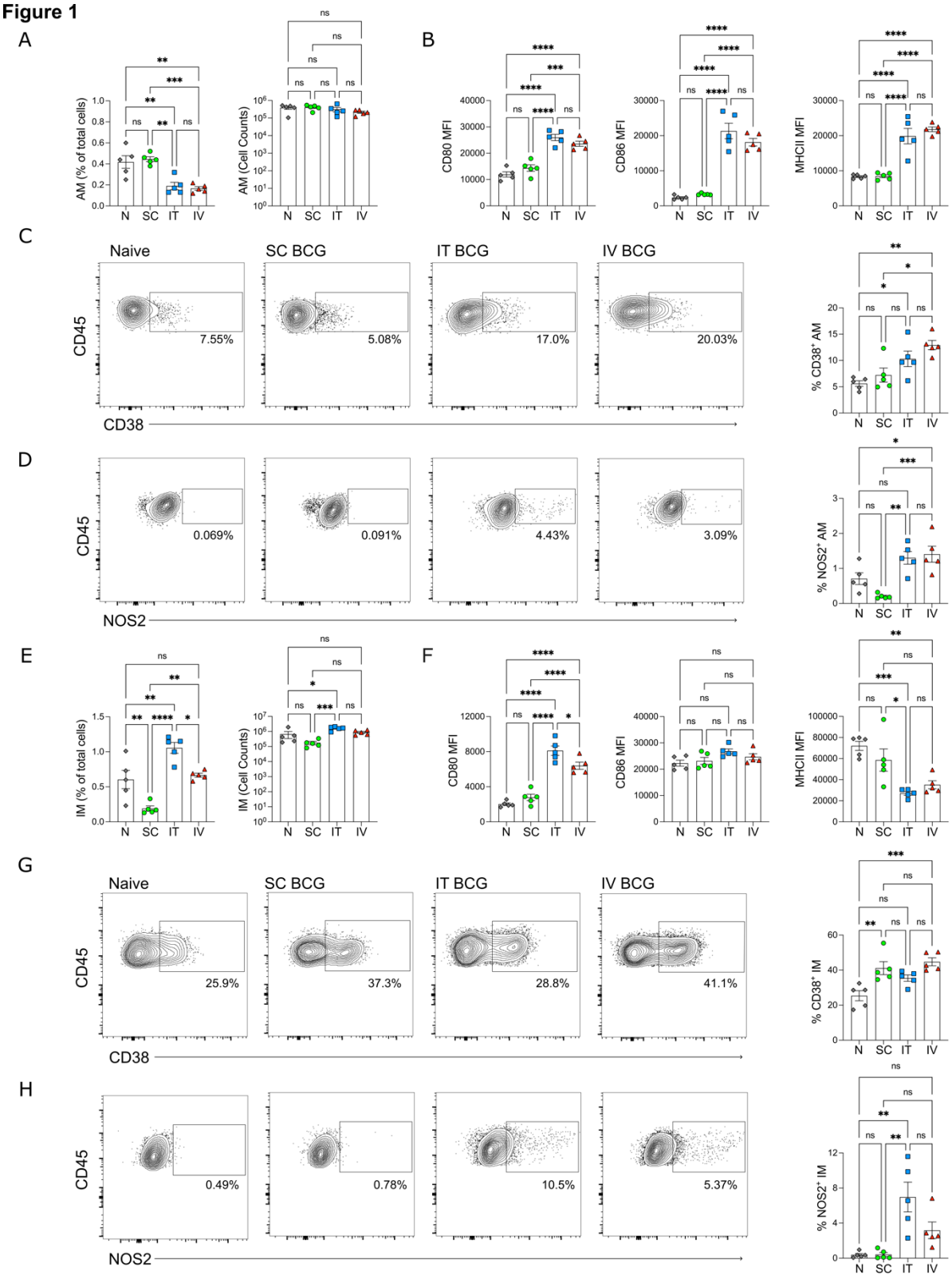

730

Figure 1: IT BCG supports enhanced IM activation.

(A): Frequency of total lung cells and absolute numbers of AM 8 weeks after SC, IT and IV BCG vaccination. **(B)**: Mean Fluorescence Intensity (MFI) of CD80, CD86 and MHCII expressed by AM after BCG vaccination. **(C, D)**: Representative plots and quantification of CD38 or NOS2 positive AM 8 weeks after BCG vaccination. **(E)**: Frequency of total lung cells and absolute numbers of IM 8 weeks after SC, IT and IV BCG vaccination. **(F)**: MFI of CD80, CD86 and MHCII on IM 8 weeks vaccination. **(G, H)**: Representative plots and quantification of CD38 or NOS2 positive IM 8 weeks after BCG vaccination. N: Each datapoint indicates one individual mouse. One-Way ANOVA with Tukey's multiple comparison test was used to determine statistical significance.

Figure S1

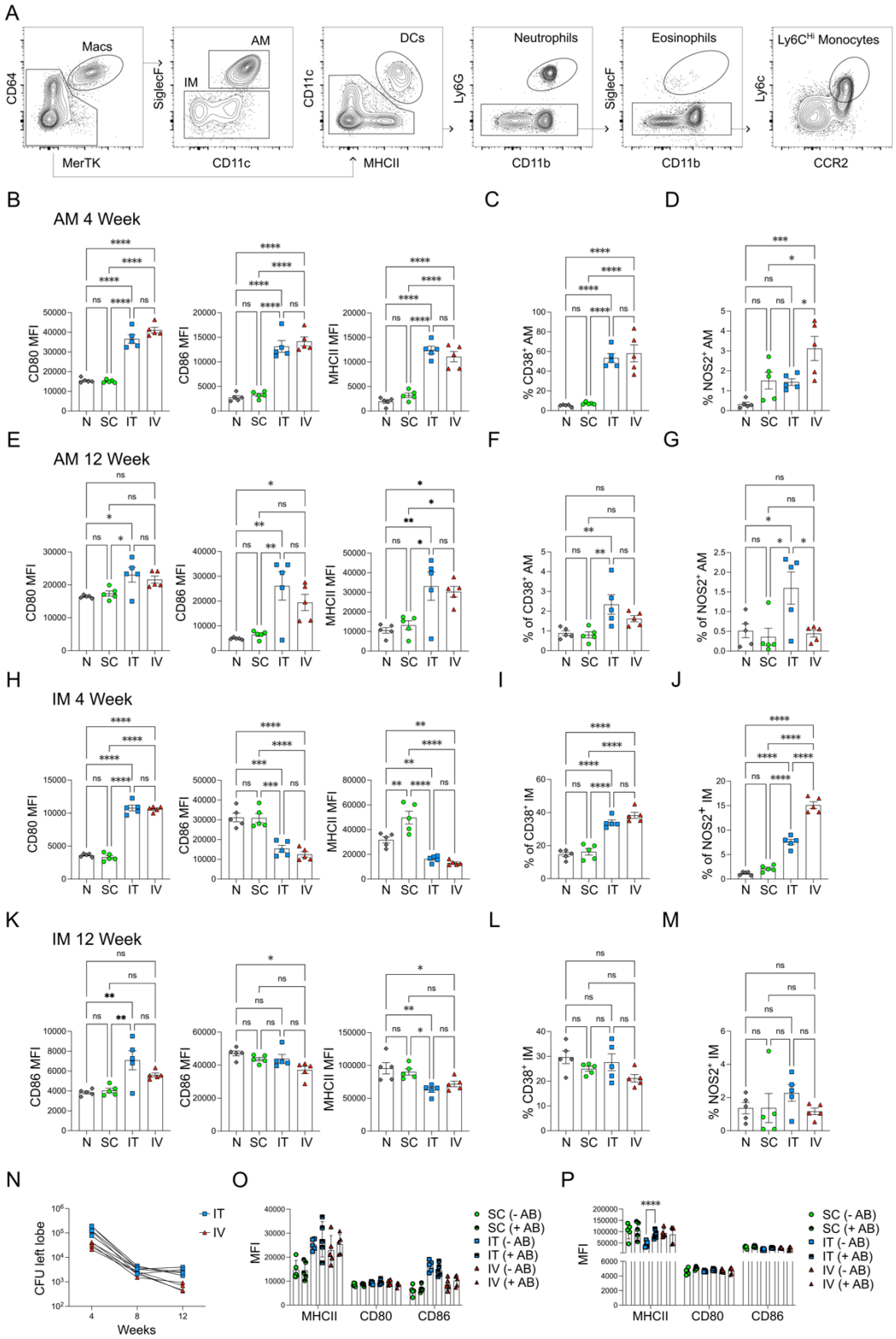
A
Macs
CD64
MerTK
AM
IM
SiglecF
CD11c
DCs
CD11c
MHCII
Neutrophils
Ly6G
CD11b
Eosinophils
SiglecF
CD11b
Ly6C^Hi Monocytes
Ly6c
CCR2
B
AM 4 Week
CD80 MFI
CD86 MFI
MHCII MFI
C
% CD38+ AM
D
% NOS2+ AM
E
AM 12 Week
F
G
H
IM 4 Week
I
J
K
IM 12 Week
L
M
% CD38+ IM
% NOS2+ IM
N
CFU left lobe
Weeks
IT
IV
O
MFI
MHCII
CD80
CD86
SC (- AB)
SC (+ AB)
IT (- AB)
IT (+ AB)
IV (- AB)
IV (+ AB)
P
N SC IT IV

765 **Supplementary Figure 1: IT BCG supports enhanced IM activation.**
766 **(A)**: Gating strategy used to identify lung innate immune cells including AM, IM, DCs,
767 neutrophils, eosinophils and Ly6C Hi monocytes. Gated on live, CD45+, CD3-, CD19- & Nkp46-
768 cells. **(B)**: MFI of CD80, CD86 and MHCII expression by AM 4 weeks after SC, IT or IV BCG
769 vaccination. **(C, D)**: Frequency of CD38 or NOS2 positive AM from mice vaccinated as in (B).
770 **(E-G)**: MFI of CD80, CD86 and MHCII expression by AM 12 weeks after vaccination (E) and
771 the frequency of CD38 or NOS2 positive cells (F, G). **(H)**: MFI of CD80, CD86 and MHCII
772 expression by IM 4 weeks after SC, IT or IV BCG vaccination. **(I, J):** Frequency of CD38 or
773 NOS2 positive IM from mice vaccinated as in (H). **(K-M)**: MFI of CD80, CD86 and MHCII
774 expression by IM 12 weeks after vaccination (K) and the frequency of CD38 or NOS2 positive
775 cells (L, M). **(N)**: BCG bacterial burden in the lungs of mice vaccinated with IT or IV BCG for 4,
776 8 and 12 weeks. **(O, P)**: MFI of MHCII, CD80 or CD86 expression by AM (O), or by IM (P), in
777 mice that had been vaccinated with BCG and subsequently treated with antibiotics. N: Each
778 datapoint indicates one individual mouse. One-Way ANOVA with Tukey's multiple comparison
779 test was used to determine statistical significance.
780
781
782
783
784
785
786
787
788
789
790
791
792
793
794
795

Figure 2

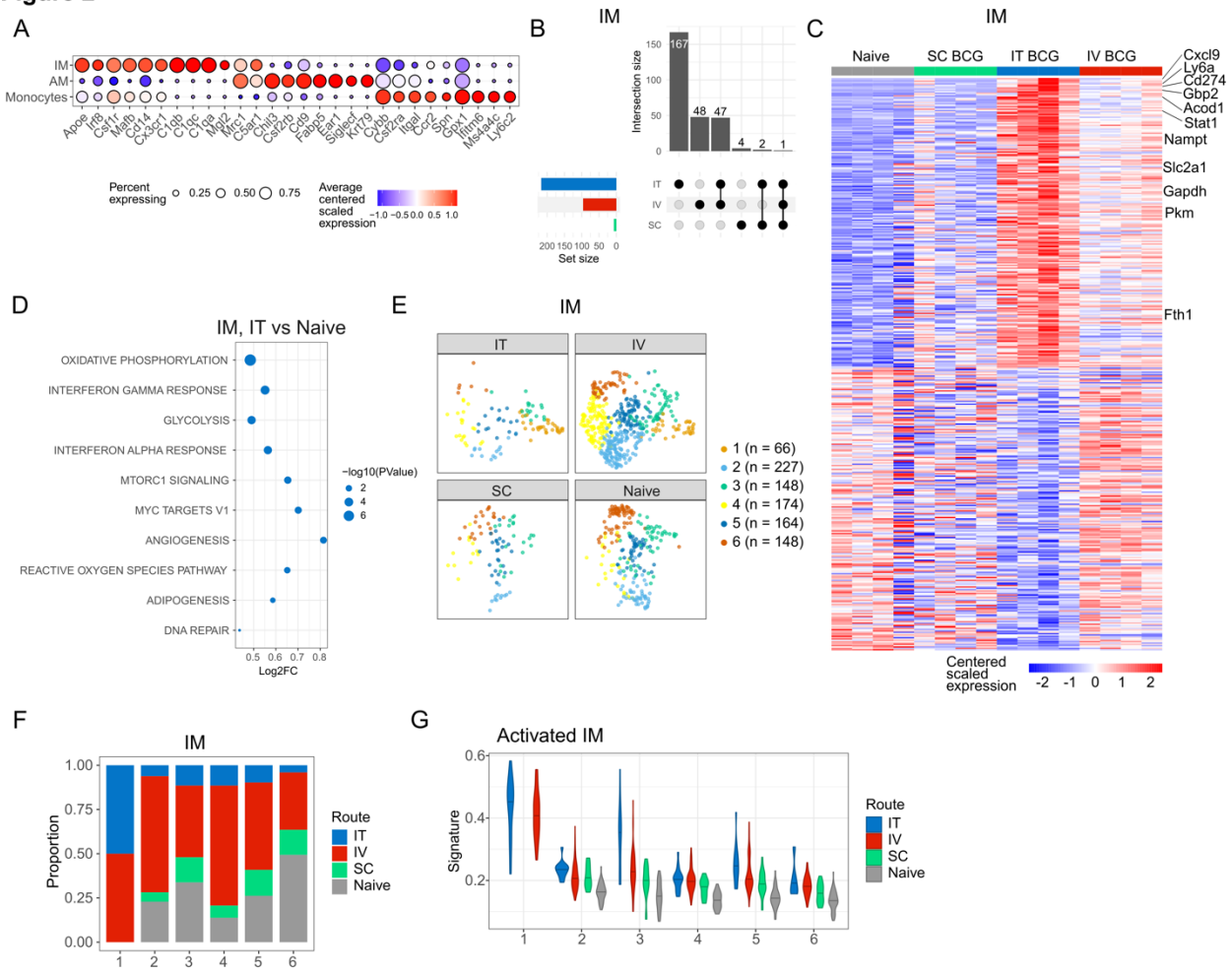

796

797

798

799 **Figure 2: IT BCG transcriptionally rewires IM.**

800 **(A):** Expression of signature genes used to identify AM, IM and monocytes in the single cell RNA-
801 Seq dataset. **(B):** Upset plot depicting the number of genes upregulated by IM after each route of
802 BCG vaccination as compared to naïve cells. **(C)**: Heatmap depicting differentially expressed
803 genes by IM following IT BCG vaccination. **(D)**: Pathway enrichment analysis performed on the
804 genes upregulated by IM 8 weeks after IT BCG vaccination. **(E):** UMAP displaying IM clusters
805 that were present in naive mice and after SC, IT or IV BCG vaccination. **(F):** Proportion of IM
806 clusters described in (E). **(G)**: Violin plot depicting the activated IM expression signature score in
807 each IM cluster.

Figure S2

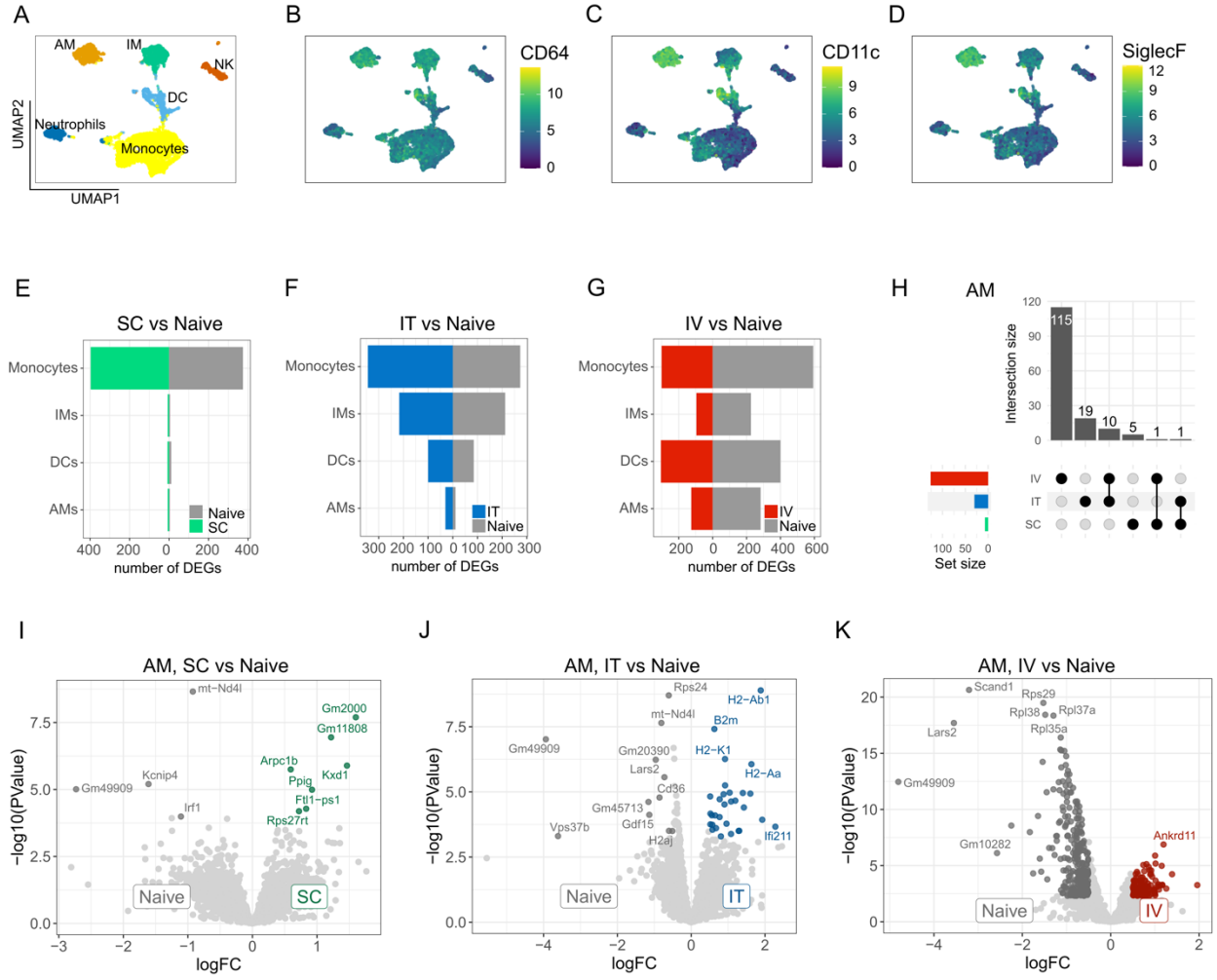

808

809

810

811 **Supplementary Figure 2: IT BCG transcriptionally rewires IM.**

812 **(A):** UMAP depicting clusters of AM, IM, DC, neutrophils and DCs identified in single cell RNA
813 Seq dataset. **(B-D):** UMAP depicting protein expression of CD64 (B), CD11c (C) and SiglecF (B).
814 **(E-G)**: Barplots depicting the number of differentially expressed genes in monocytes, DCs, IM or
815 AM 8 weeks after SC, IT or IV BCG vaccination. **(H)**: Upset plot depicting the number of genes
816 upregulated by AM after each route of BCG vaccination as compared to naïve cells. **(I-K)**: Volcano
817 plots depicting genes expressed by AM following SC (I), IT (J) or IV (K) vaccination. Coloured
818 dots represent significantly differentially expressed genes with FDR < 0.05 and |logFC| > 0.5 (dark
819 grey for Naive, green for BCG SC, blue for BCG IT, red for BCG IV). Light grey dots represent
820 non-significant genes.

821

Figure 3

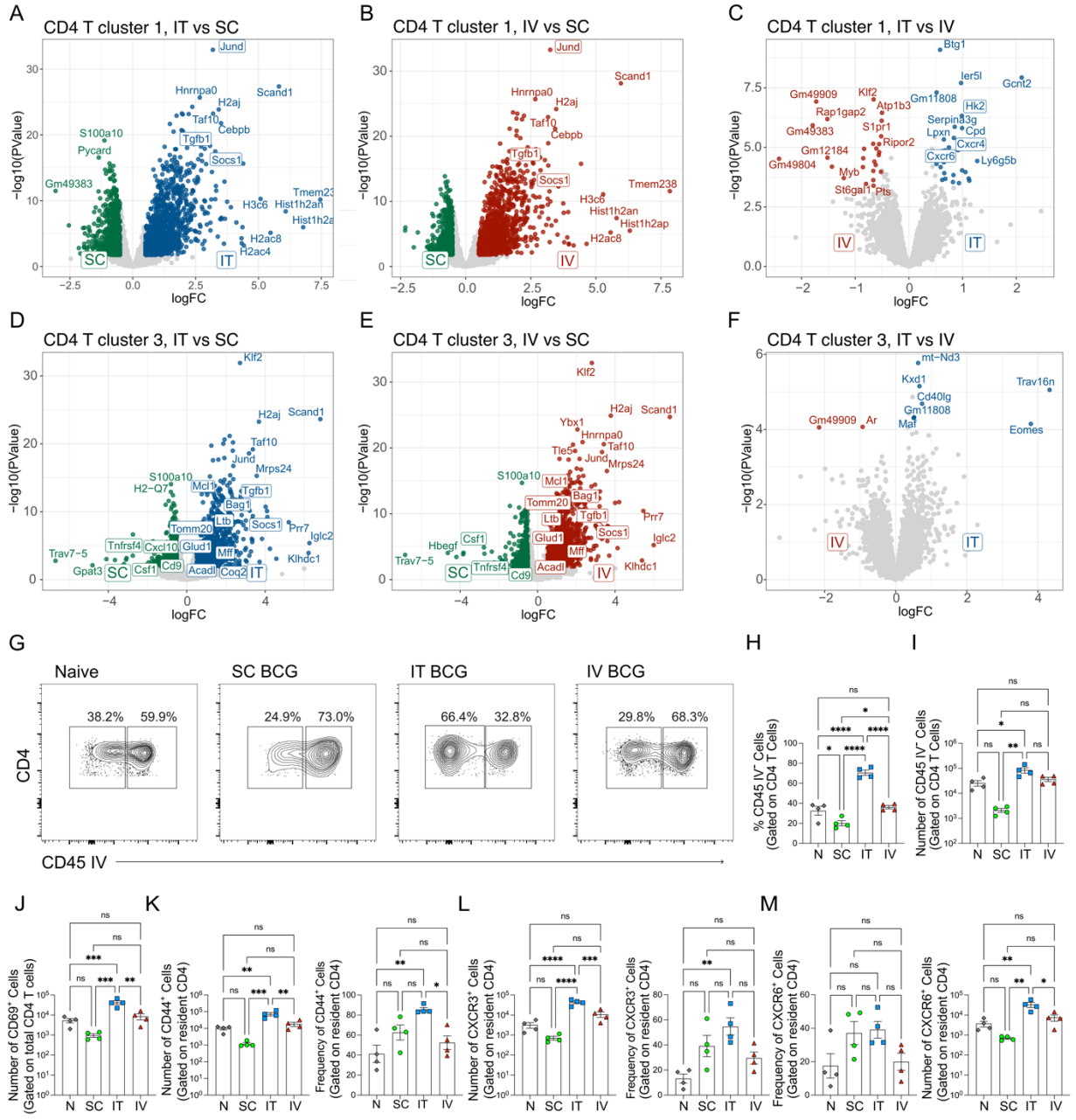

822

823

824

825 **Figure 3: CD4 T cells likely produce IFNγ after all routes of BCG vaccination.**
826 **(A-C)**: Volcano plots depicting DEGs in cluster 1 CD4 T cells IT vs SC (A), IV vs SC (B) or IT
827 vs IV (C). **(D-F)**: Volcano plots depicting DEGs in cluster 3 CD4 T cells IT vs SC (D), IV vs SC
828 (E) or IT vs IV (F). **(G)**: Representative plots depicting the proportions of CD45 IV positive and
829 negative CD4 T cells in naive mice or in animals vaccinated with SC IT or IV BCG 8 weeks prior.
830 **(H, I)**: Frequency (H) and absolute number (I) of CD45 negative CD4 T cells in naive and
831 vaccinated mice. **(J)**: Number of CD69 positive resident CD4 T cells in naive mice and those
832 vaccinated 8 weeks prior. **(K-M)**: Frequency and absolute numbers of CD45 negative CD4 T cells
833 expressing CD44 (K), CXCR3 (L) and CXCR6 (M). For Fig. 3 H-M, N: Each datapoint indicates
834 one individual mouse. One-Way ANOVA with Tukey's multiple comparison test was used to
835 determine statistical significance. For volcano plots the coloured dots represent significantly
836 differentially expressed genes with FDR < 0.05 and $|\log FC| > 0.5$ (dark grey for Naive, green for
837 BCG SC, blue for BCG IT, red for BCG IV). Light grey dots represent non-significant genes.
838

Figure S3

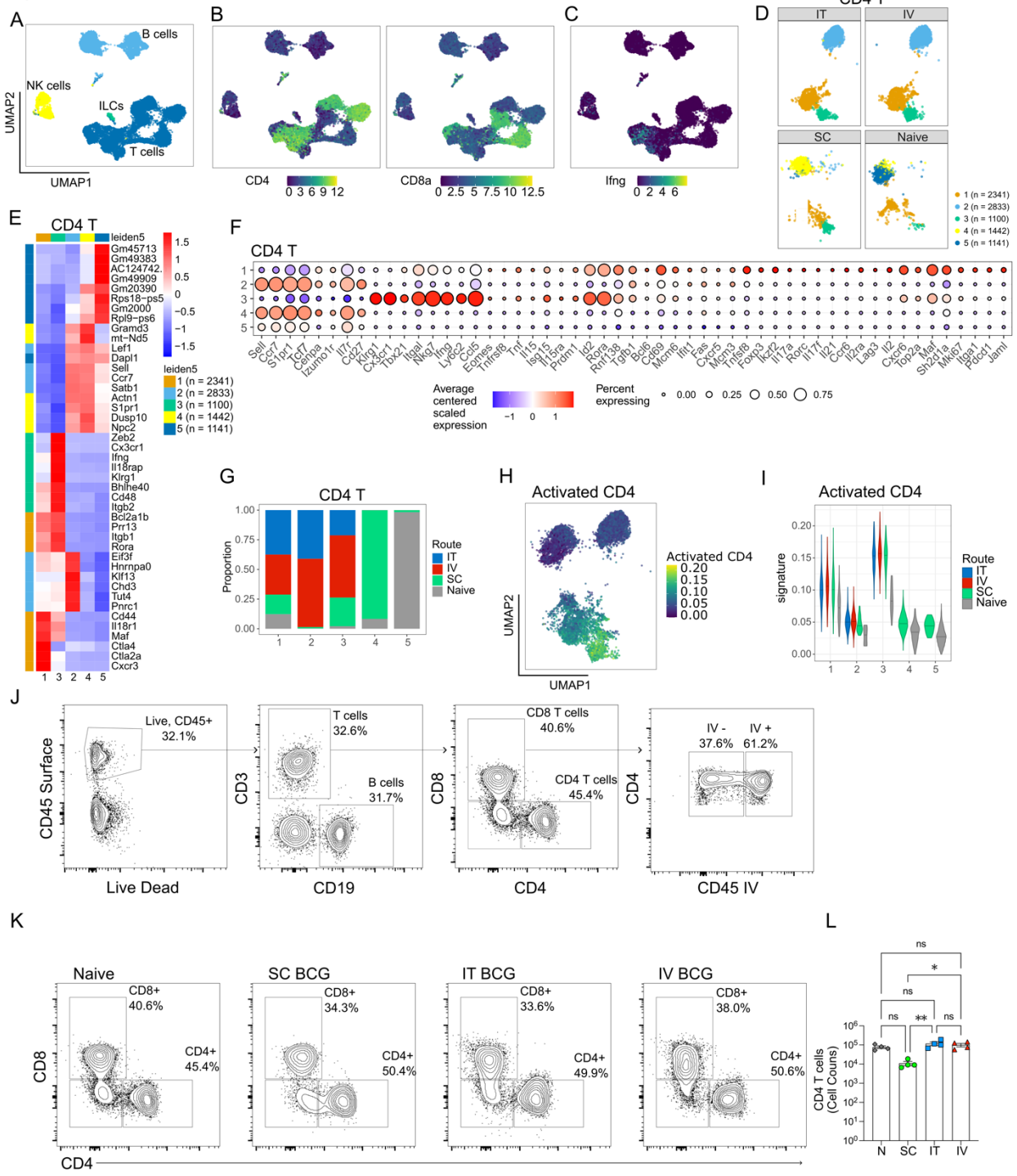

839

840

841

842 **Supplementary Figure 3: CD4 T cells likely produce IFNγ after all routes of BCG**
843 **vaccination.**
844 **(A, B):** UMAP depicting lymphocyte populations identified in single cell RNA Seq (A) and
845 Protein expression of CD4 and CD8 (B). **(C):** Expression of IFNgamma by the lymphocyte
846 populations identified in (A). **(D)**: Clusters of CD4 T cells identified 8 weeks after SC, IT and IV
847 BCG vaccination. **(E, F)**: Heatmap with the top 10 genes expressed by each cluster of CD4 T cells
848 (E) and the expression of marker genes (F) used to identify the CD4 subsets. **(G)**: Proportion of
849 each cluster of CD4 T cells 8 weeks after SC, IT and IV BCG vaccination. **(H)**: Expression of the
850 activated CD4 signature score on the clusters of CD4 T cells. **(I)**: Violin plot depicting the strength
851 of the activated CD4 expression signature in each CD4 T cell cluster. **(J)**: Gating strategy used to
852 identify CD4 T cells. **(K, L)**: Representative plots and cell counts of CD4 T cells in naive and
853 BCG vaccinated mice. For L, N: Each datapoint indicates one individual mouse. One-Way
854 ANOVA with Tukey's multiple comparison test was used to determine statistical significance.

Figure 4

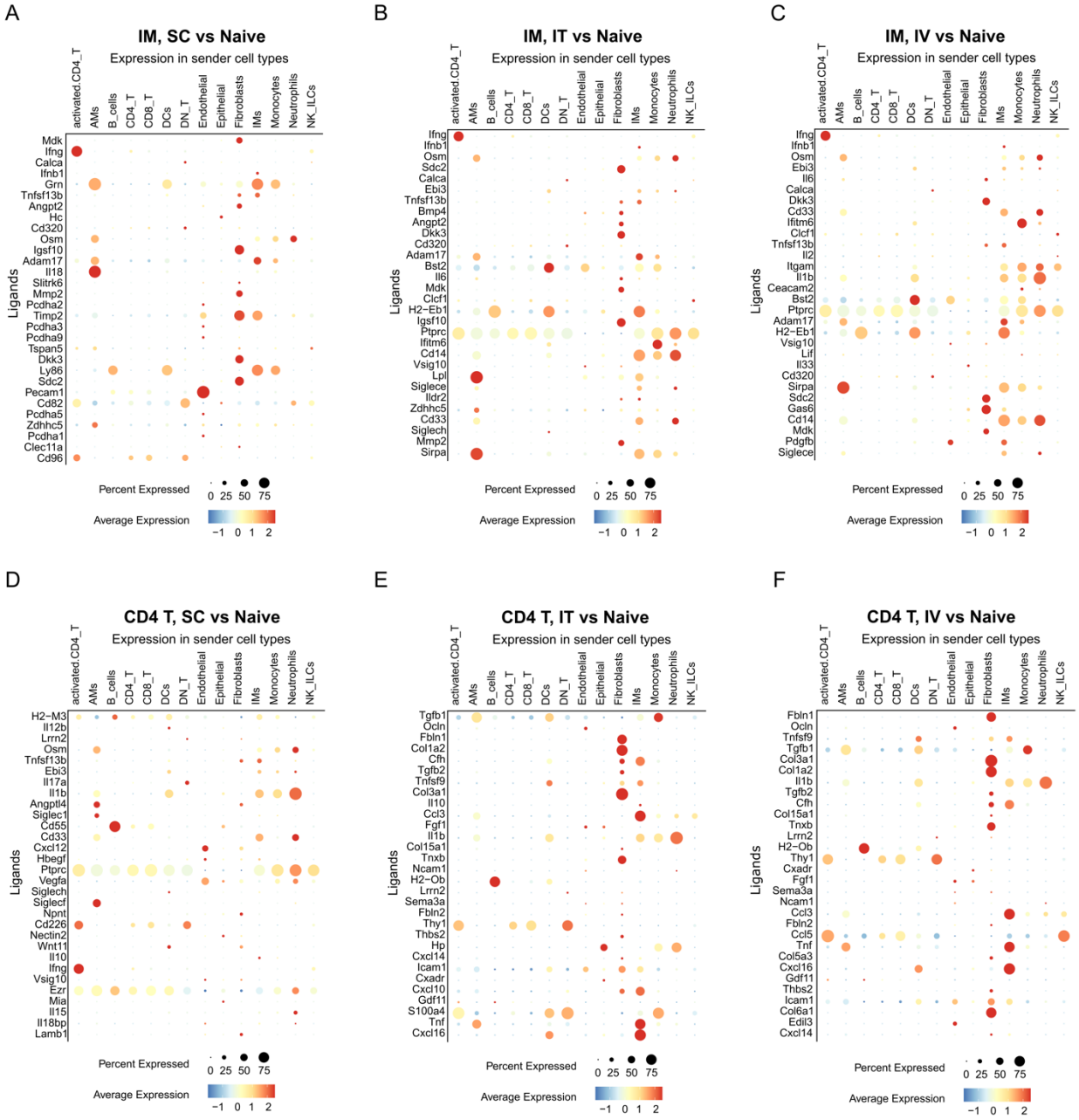
A
IM, SC vs Naive
Expression in sender cell types
activated.CD4_T
AMs
B_cells
CD4_T
CD8_T
DCs
DN_T
Endothelial
Epithelial
Fibroblasts
IMs
Monocytes
Neutrophils
NK_ILCs
Ligands
Mdk
Ifng
Calca
Ifnb1
Grn
Tnfsf13b
Angpt2
Hc
Cd320
Osm
Igsf10
Adam17
Il18
Slitrk6
Mmp2
Pcdha2
Timp2
Pcdha3
Pcdha9
Tspan5
Dkk3
Ly86
Sdc2
Pecam1
Cd82
Pcdha5
Zdhhc5
Pcdha1
Clec11a
Cd96
Percent Expressed
0 25 50 75
Average Expression
−1 0 1 2
B
IM, IT vs Naive
Expression in sender cell types
Ifng
Ifnb1
Osm
Sdc2
Calca
Ebi3
Tnfsf13b
Bmp4
Angpt2
Dkk3
Cd320
Adam17
Bst2
Il6
Mdk
Clcf1
H2−Eb1
Igsf10
Ptprc
Ifitm6
Cd14
Vsig10
Lpl
Siglece
Ildr2
Zdhhc5
Cd33
Siglech
Mmp2
Sirpa
C
IM, IV vs Naive
Expression in sender cell types
Ifng
Ifnb1
Osm
Ebi3
Il6
Calca
Dkk3
Cd33
Ifitm6
Clcf1
Tnfsf13b
Il2
Itgam
Il1b
Ceacam2
Bst2
Ptprc
Adam17
H2−Eb1
Vsig10
Lif
Il33
Cd320
Sirpa
Sdc2
Gas6
Cd14
Mdk
Pdgfb
Siglece
D
CD4 T, SC vs Naive
Expression in sender cell types
H2−M3
Il12b
Lrrn2
Osm
Tnfsf13b
Ebi3
Il17a
Il1b
Angptl4
Siglec1
Cd55
Cd33
Cxcl12
Hbegf
Ptprc
Vegfa
Siglech
Siglecf
Npnt
Cd226
Nectin2
Wnt11
Il10
Ifng
Vsig10
Ezr
Mia
Il15
Il18bp
Lamb1
E
CD4 T, IT vs Naive
Expression in sender cell types
Tgfb1
Ocln
Fbln1
Col1a2
Cfh
Tgfb2
Tnfsf9
Col3a1
Il10
Ccl3
Fgf1
Il1b
Col15a1
Tnxb
Ncam1
H2−Ob
Lrrn2
Sema3a
Fbln2
Thy1
Thbs2
Hp
Cxcl14
Icam1
Cxadr
Cxcl10
Gdf11
S100a4
Tnf
Cxcl16
F
CD4 T, IV vs Naive
Expression in sender cell types
Fbln1
Ocln
Tnfsf9
Tgfb1
Col3a1
Col1a2
Il1b
Tgfb2
Cfh
Col15a1
Tnxb
Lrrn2
H2−Ob
Thy1
Cxadr
Fgf1
Sema3a
Ncam1
Ccl3
Fbln2
Ccl5
Tnf
Col5a3
Cxcl16
Gdf11
Thbs2
Icam1
Col6a1
Edil3
Cxcl14

858 **Figure 4: IM-CD4 T cell crosstalk following BCG Vaccination.**

859 **(A-C)**: NicheNet analysis showing the expression of ligands received by IM (compared to Naive)
860 in the sender cell type after each route of vaccination. **(D-F)**: NicheNet analysis showing the
861 expression of ligands received by CD4 T cells (compared to Naive) in the sender cell type after
862 each route of vaccination.

Figure S4

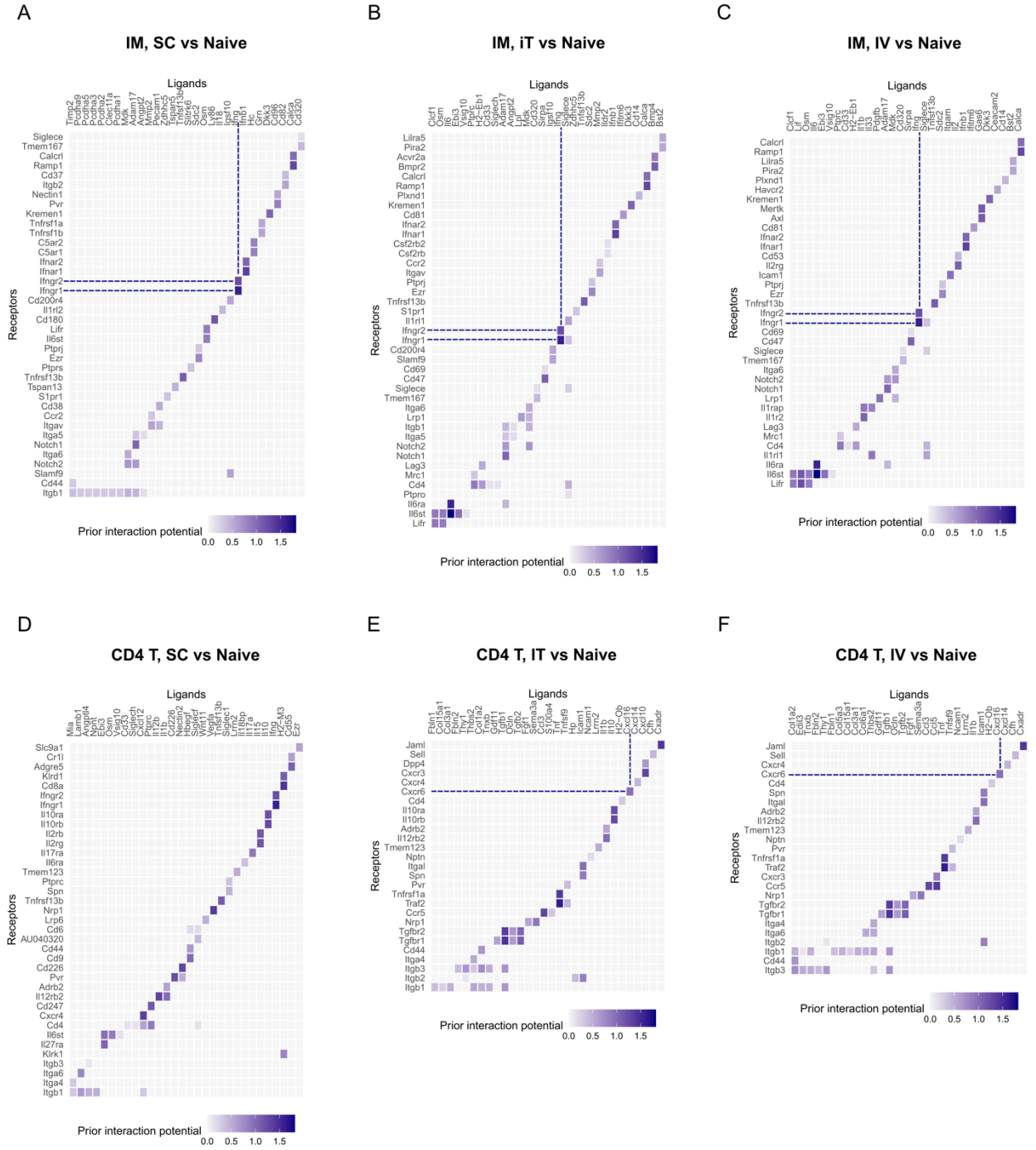

863

864

865

866 **Supplementary Figure 4: IM-CD4 T cell crosstalk following BCG Vaccination.**
867 **(A):** Heatmap representing NicheNet-predicted interaction potentials for ligand-receptor pairs,
868 between the sender cell types and IM, that are contributing to downstream differentially
869 expressed genes identified comparing BCG SC vs Naïve, BCG IT vs Naïve **(B)** and BCG IV vs
870 Naïve **(C)**. The interaction between *Ifng* and *Ifngr1*/*Ifngr2* is highlighted. **(D):** Heatmap
871 representing NicheNet-predicted interaction potentials for ligand-receptor pairs, between the
872 sender cell types and CD4 T cells, that are contributing to downstream differentially expressed
873 genes identified comparing BCG SC vs Naïve, BCG IT vs Naïve **(E)** and BCG IV vs Naïve **(F)**.
874 The interactions between Ifng and *Ifngr1*/*Ifngr2* and between Cxcl16 and Cxcr6 are highlighted.
875

Figure 5

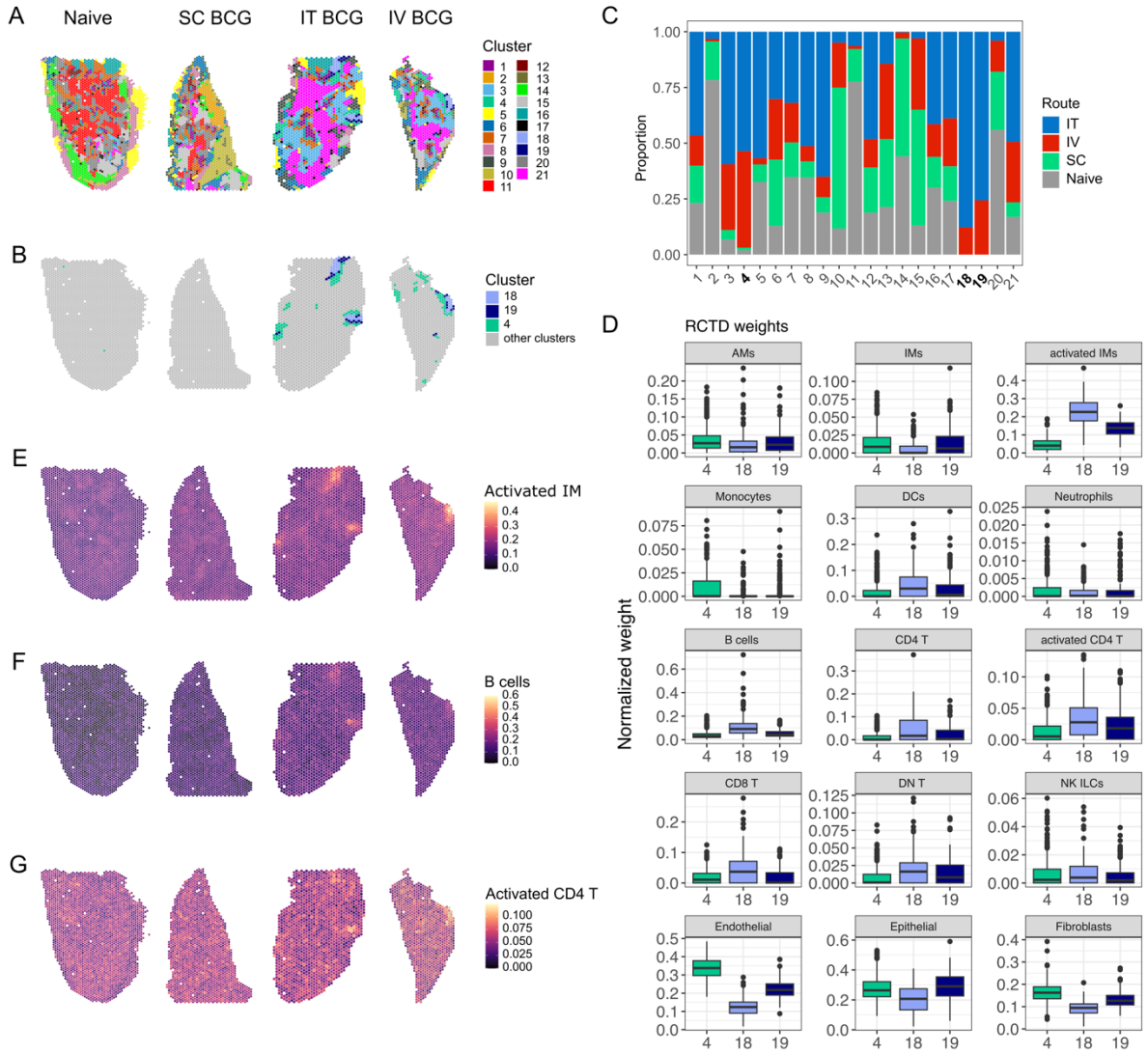
A
Naive
SC BCG
IT BCG
IV BCG
Cluster
B
Cluster
18
19
4
other clusters
E
Activated IM
F
B cells
G
Activated CD4 T
C
Proportion
Route
IT
IV
SC
Naive
D
RCTD weights
AMs
IMs
activated IMs
Monocytes
DCs
Neutrophils
B cells
CD4 T
activated CD4 T
CD8 T
DN T
NK ILCs
Endothelial
Epithelial
Fibroblasts
Normalized weight

879 **Figure 5: Activated IM localise in distinct tissue niches within the lung.**
880 **(A):** Spatial images depicting the clusters identified in naïve mice and animals that had been
881 vaccinated 8 weeks previously. **(B):** Spatial images depicting only clusters 4, 18 and 19 in IT and
882 IV BCG vaccinated samples. **(C):** The proportion of each cluster following each route of
883 vaccination as well as in naive conditions. **(D):** RCTD weight plots of the immune and non immune
884 cells present in cluster 4, 18 and 19. **(E-G)**: Overlay of activated IM (E), B cell (F) and activated
885 CD4 (G) expression signature scores onto spatial slices taken from the lung of mice vaccinated 8
886 weeks prior as well as from naive animals.

Figure S5

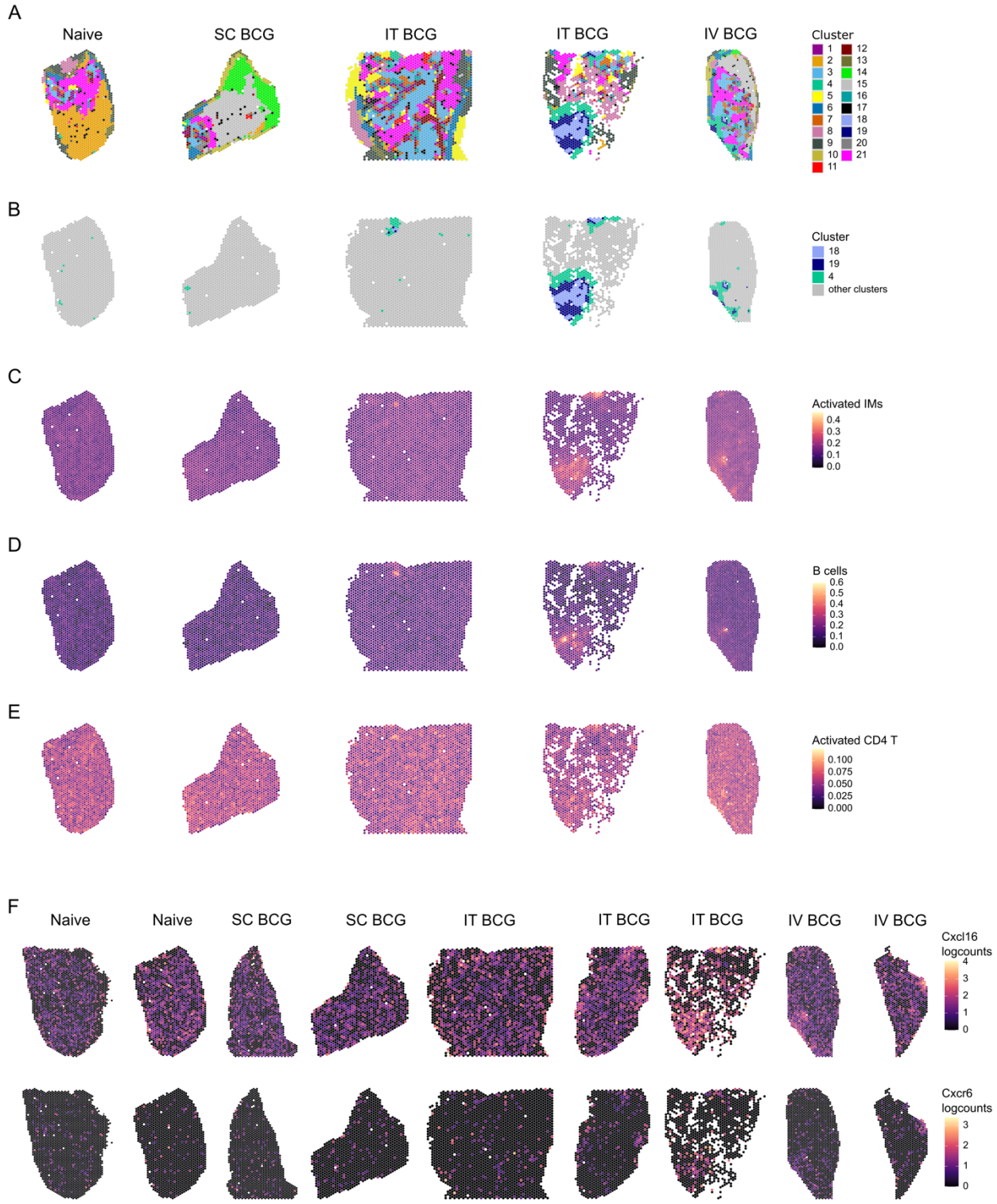
A
Naive
SC BCG
IT BCG
IT BCG
IV BCG
Cluster
1 2 3 4 5 6 7 8 9 10 11 12 13 14 15 16 17 18 19 20 21
B
Cluster
18
19
4
other clusters
C
Activated IMs
0.4 0.3 0.2 0.1 0.0
D
B cells
0.6 0.5 0.4 0.3 0.2 0.1 0.0
E
Activated CD4 T
0.100 0.075 0.050 0.025 0.000
F
Naive
Naive
SC BCG
SC BCG
IT BCG
IT BCG
IT BCG
IV BCG
IV BCG
Cxcl16
logcounts
4 3 2 1 0
Cxcr6
logcounts
3 2 1 0

890 **Supplementary Figure 5: Activated IM localise in distinct tissue niches within the lung.**
891 **(A):** Spatial images of additional samples, depicting the clusters identified in naïve mice and
892 animals that had been vaccinated 8 weeks previously. **(B)**: Spatial images of additional samples,
893 depicting only clusters 4, 18 and 19 in IT and IV BCG vaccinated samples. **(C-E):** Overlay of
894 activated IM (C), B cells (D) and activated CD4 T cells (F) expression signature scores onto
895 additional spatial slices taken from the lung of mice vaccinated 8 weeks prior as well as from naive
896 animals. **(F):** *Cxcl16* (top) and *CxCr6* (bottom) gene expression on all spatial
897 slices taken from the lung of naive animals as well as from mice vaccinated 8
898 weeks prior.
899
900

Figure 6

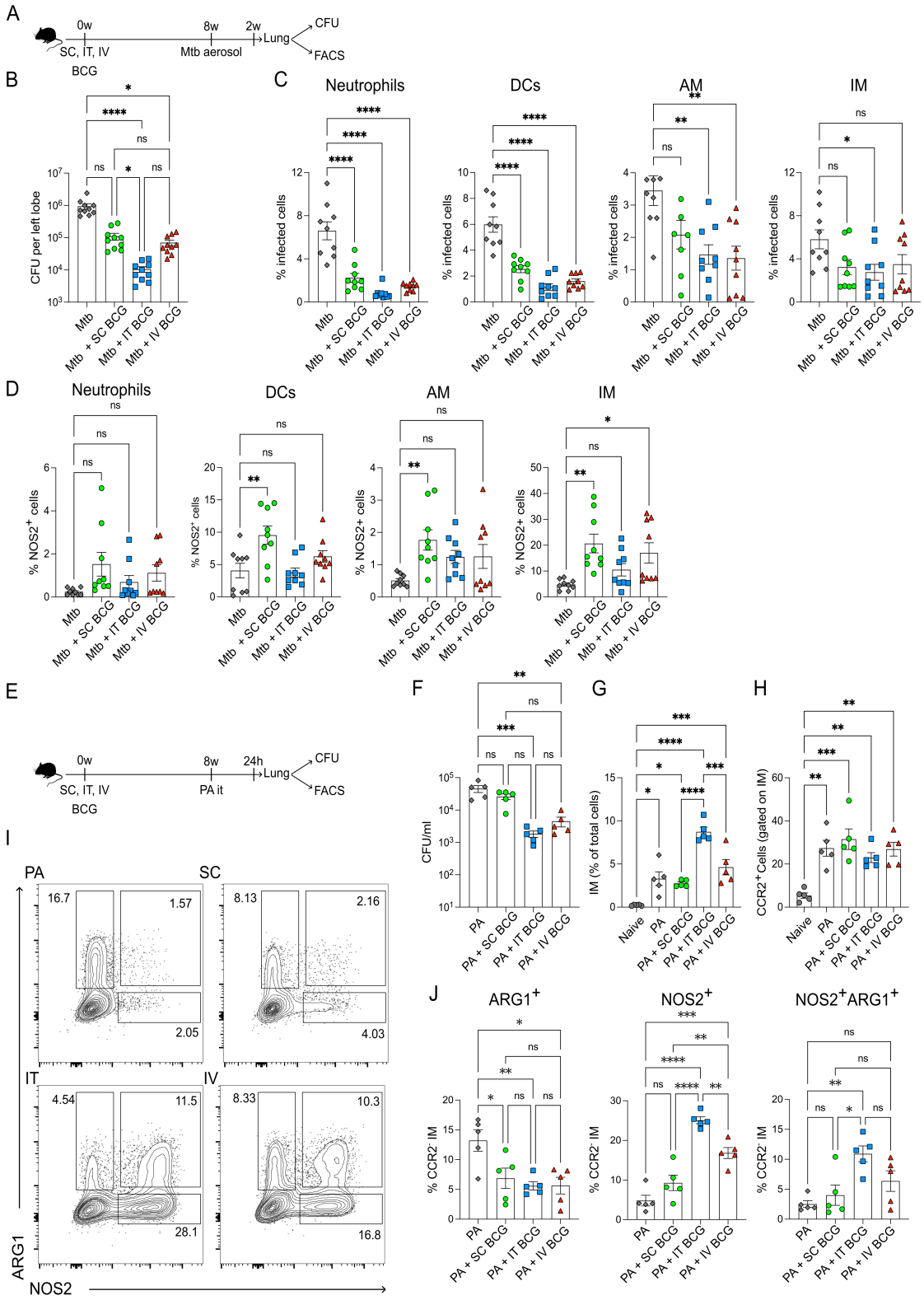
A
0w
8w
2w
Lung
CFU
FACS
SC, IT, IV
BCG
Mtb aerosol
B
CFU per left lobe
Mtb
Mtb + SC BCG
Mtb + IT BCG
Mtb + IV BCG
C
Neutrophils
DCs
AM
IM
% infected cells
D
% NOS2+ cells
E
0w
8w
24h
Lung
CFU
FACS
SC, IT, IV
BCG
PA it
F
CFU/ml
PA
PA + SC BCG
PA + IT BCG
PA + IV BCG
G
IM (% of total cells)
Naive
H
CCR2+Cells (gated on IM)
I
PA
SC
IT
IV
ARG1
NOS2
J
ARG1+
NOS2+
NOS2+ARG1+
% CCR2- IM

904 **Figure 6: IT BCG vaccination confers superior protection during Mtb challenge.**
905 (**A):** Schematic depicting the experimental set up of the Mtb rechallenge. **(B)**: Quantification of
906 Mtb bacterial burden 2 weeks after aerosol infection in unvaccinated mice or in animals that had
907 received SC, IT or IV BCG vaccination 8 weeks previously. **(C):** Frequency of infected
908 neutrophils, dendritic cells, AM and IM. **(D):** Bar plots depicting frequency of NOS2 positive
909 neutrophils, DCs, AM and IM. **(E)**: Schematic depicting the experimental set up of the PA
910 rechallenge. **(F)**: Quantification of PA burden 24 hours after infection in unvaccinated mice or in
911 animals that had received SC, IT or IV BCG vaccination 8 weeks previously. **(G)**: Frequency of
912 IM following PA infection as in (F). **(H)**: Quantification of CCR2 positive IM following PA
913 infection. **(I)**: Representative FACs plots depicting Arg1 positive, NOS2 positive or double
914 positive CCR2 negative IM. **(J)**: Quantification of Arg1 positive, NOS2 positive and double
915 positive IM after PA infection. N: Each datapoint indicates one individual mouse. For B: One-
916 Way ANOVA with non-parametric Kruskal-Wallis Test was performed. For C-J: One-Way
917 ANOVA with Tukey's multiple comparison test was used to determine statistical significance.

Figure S6

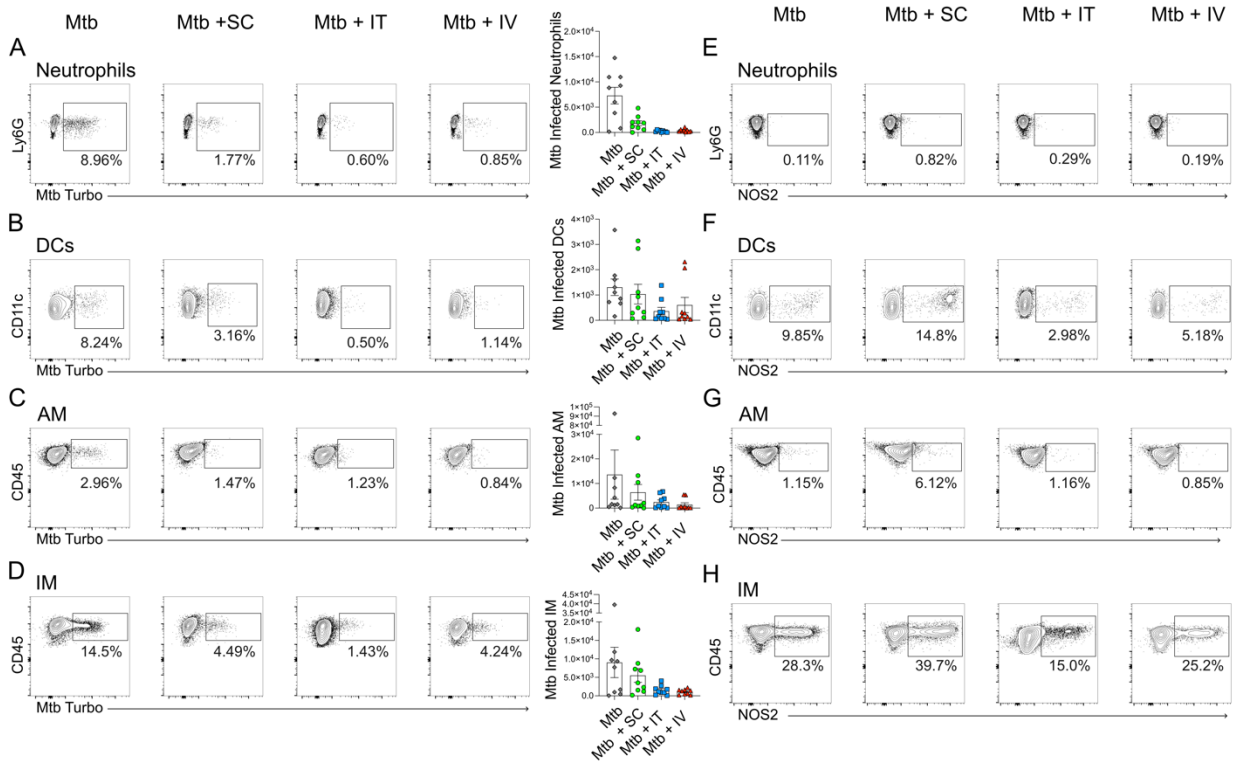

918

919

920

921 **Supplementary Figure 6: IT BCG vaccination confers superior protection during Mtb**
922 **challenge.**
923 **(A-D)**: Representative FACS plots depicting Mtb-turbo signal in neutrophils (A), DCs (B), AM
924 (C) and IM (D). Bar plots depict the number of infected cells for each condition. **(E-H)**:
925 Representative FACs plots depicting NOS2 expression in neutrophils (E), DCs (F), AM (G) and
926 IM (H).
927